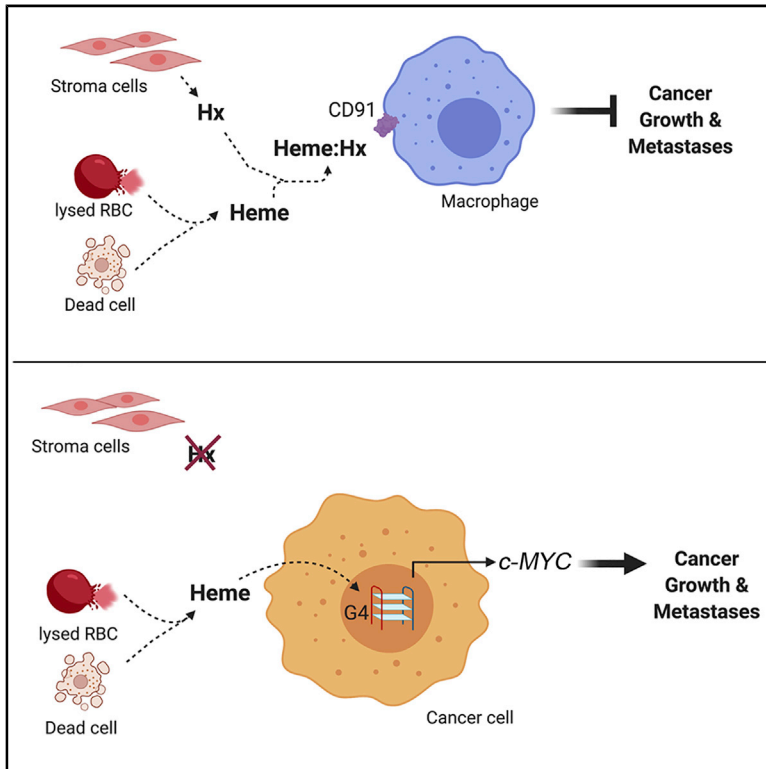# Scavenging of Labile Heme by Hemopexin Is a Key Checkpoint in Cancer Growth and Metastases

Graphical Abstract

Authors

Giacomo Canesin, Annalisa Di Ruscio, Mailin Li, ..., Anders Bjartell, Daniel G. Tenen, Barbara Wegiel

Correspondence

adirusci@bidmc.harvard.edu (A.D.R.), bwegiel@bidmc.harvard.edu (B.W.)

In Brief

Canesin et al. describe a role and mechanism for labile heme as a key player in regulating gene expression to promote carcinogenesis via binding to G-quadruplex in the *c-MYC* promoter. Hemopexin, a heme scavenger, may be used as a strategy to block progression of cancer.

Highlights

- Stroma-expressed hemopexin (Hx) correlates with a better prostate cancer prognosis

- Lack of Hx in the stroma promotes malignant phenotype and tumor dissemination

- Labile heme accumulates in the nucleus and promotes cancer cell growth *in vitro*

- Heme modulates *c-MYC* expression by binding to G-quadruplex structures in its promoter

Article

Scavenging of Labile Heme by Hemopexin Is a Key Checkpoint in Cancer Growth and Metastases

Giacomo Canesin,[1,11] Annalisa Di Ruscio,[2,3,9,10,11,*] Mailin Li,[1,3,12] Simone Ummarino,[2,3,12] Andreas Hedblom,[1,12] Reeham Choudhury,[1] Agnieszka Krzyzanowska,[4] Eva Csizmadia,[1] Macarena Palominos,[4] Anna Stiehm,[4] Alexander Ebralidze,[2] Shao-Yong Chen,[2] Mahmoud A. Bassal,[2] Ping Zhao,[5] Emanuela Tolosano,[6] Laurence Hurley,[5] Anders Bjartell,[4] Daniel G. Tenen,[7,8] and Barbara Wegiel[1,9,13,*]

[1]Department of Surgery, Division of Surgical Oncology, Beth Israel Deaconess Medical Center, Harvard Medical School, Boston, MA 02214, USA
[2]Department of Medicine, Beth Israel Deaconess Medical Center, Harvard Medical School, Boston, MA 02214, USA
[3]University of Eastern Piedmont, Department of Translational Medicine, Novara, Italy
[4]Department of Translational Medicine, Division of Urological Cancers, Lund University, Malmo, Sweden
[5]College of Pharmacy, University of Arizona, Tucson, AZ 85721, USA
[6]Department of Molecular Biotechnology and Health Sciences, University of Torino, Torino, Italy
[7]Cancer Science Institute of Singapore, Singapore
[8]Harvard Stem Cell Institute, Harvard Medical School, Cambridge, MA 02138, USA
[9]Cancer Research Institute, Beth Israel Deaconess Medical Center, Harvard Medical School, Boston, MA 02214, USA
[10]HMS Initiative for RNA Medicine, Beth Israel Deaconess Medical Center, Harvard Medical School, Boston, MA 02214, USA
[11]These authors contributed equally
[12]These authors contributed equally
[13]Lead Contact
*Correspondence: adirusci@bidmc.harvard.edu (A.D.R.), bwegiel@bidmc.harvard.edu (B.W.)
https://doi.org/10.1016/j.celrep.2020.108181

SUMMARY

Hemopexin (Hx) is a scavenger of labile heme. Herein, we present data defining the role of tumor stroma-expressed Hx in suppressing cancer progression. Labile heme and Hx levels are inversely correlated in the plasma of patients with prostate cancer (PCa). Further, low expression of Hx in PCa biopsies characterizes poorly differentiated tumors and correlates with earlier time to relapse. Significantly, heme promotes tumor growth and metastases in an orthotopic murine model of PCa, with the most aggressive phenotype detected in mice lacking Hx. Mechanistically, labile heme accumulates in the nucleus and modulates specific gene expression via interacting with guanine quadruplex (G4) DNA structures to promote PCa growth. We identify *c-MYC* as a heme:G4-regulated gene and a major player in heme-driven cancer progression. Collectively, these results reveal that sequestration of labile heme by Hx may block heme-driven tumor growth and metastases, suggesting a potential strategy to prevent and/or arrest cancer dissemination.

INTRODUCTION

Heme is a high-energy prosthetic group of hemoproteins, whose functions range from transcription factors (i.e., neuronal PAS domain protein 2 [NPAS]), gas carriers (i.e., hemoglobin), and cytochromes to redox enzymes (Dutra and Bozza, 2014; Wegiel et al., 2015). Labile heme traffics between the cytosolic and nuclear compartments (Hanna et al., 2016; Yuan et al., 2016; Soares and Hamza, 2016). The uptake of hemoglobin or labile heme is provided by myeloid cell receptors CD163 or CD91/LRP1 by binding hemoglobin:haptoglobin (Hp) or heme:hemopexin (Hx) complexes, respectively (Hvidberg et al., 2005; Kristiansen et al., 2001). Hx has picomolar affinity toward heme; thus, any changes in its levels lead to abnormalities in heme clearance. Hx role is critical during hemolysis and heme-associated pathologies, such as sepsis, sickle cell disease, or atherosclerosis. However, there are no reports, to our knowledge, on the role of Hx in cancer. Clinically, colon cancer (in which gastrointestinal bleeds are common) or other cancers (i.e., endometriosis-associated ovarian cancer) are directly exposed to red blood cell (RBC) lysis because of bleeding and thus to hemoglobin and labile heme. The relevance of hemolysis to any cancer type is high because of excessive angiogenesis and/or intra-tumoral hemorrhage and metastatic spread.

Elevated labile heme is a characteristic of malaria (Ferreira et al., 2008), sickle cell disease (Ferreira et al., 2011), and porphyrias (Straka et al., 1990). Interestingly, individuals with malaria have higher incidence of cancer (Lehrer, 2010), indicating a possible role of heme in carcinogenesis. Heme induces hyperproliferation and the appearance of aberrant atypical and

mucosa-depleted foci in the large intestine (van der Meer-van Kraaij et al., 2005). Increased intake of red meat and thus high levels of heme in the intestinal tract may promote colonic inflammation and damage associated with a higher risk of colon cancer (Takachi et al., 2011). However, the role of labile heme in cancer and normal biology beyond its oxidant properties remains unclear (Glei et al., 2006).

Previous work suggests that the heme porphyrin ring intercalates into G-quadruplex (G4) DNA structures, affecting their stability and function (Poon et al., 2011; Saito et al., 2012a, 2012b; Sen and Poon, 2011; Shibata et al., 2016; Yamamoto et al., 2015). G4s are DNA and RNA non-canonical structures held together by guanine base quartets and stabilized by specific cations (Kosman and Juskowiak, 2016; Shumayrikh et al., 2015; Zhang et al., 2016). Moreover, G4 DNA can sequester labile heme to form DNA:heme complexes, which act as DNAzymes, exhibiting robust peroxidase and peroxygenase activities (Sen and Poon, 2011; Travascio et al., 1999). These enzymatic activities of G4:heme complexes because of their high reactivity of the iron have been studied *in vitro*, but no functional studies on the these complexes have, to our knowledge, been reported (Gray et al., 2019). G4 DNA motifs accumulate within transcriptionally active euchromatin regions (Hänsel-Hertsch et al., 2016) and coincide with critical regulatory regions of the genome, including telomeres and oncogene promoters (i.e., *c-MYC*) (Brooks and Hurley, 2010; Brooks et al., 2010). As such, these structures are known to have a role in many cellular processes regulating DNA replication and controlling gene expression (Biffi et al., 2014a; Eddy et al., 2011; Gray et al., 2014; Guo and Bartel, 2016; Hänsel-Hertsch et al., 2016; McLuckie et al., 2013; Murat and Balasubramanian, 2014; Rodriguez et al., 2012; Siddiqui-Jain et al., 2002). As an example, the nuclease hypersensitive element III1 (NHE III1), located upstream of the *c-MYC* promoter, contains G4 DNA motifs that act as transcription repressors regulating ~80% of *c-MYC* expression (Ambrus et al., 2005; Siddiqui-Jain et al., 2002). Therefore, G4s are considered to be ideal targets for anti-tumor drug development, and several ligands are being developed and tested for therapeutic approaches (Balasubramanian et al., 2011; Biffi et al., 2014a; Drygin et al., 2009; Guo and Bartel, 2016; Hänsel-Hertsch et al., 2016; McLuckie et al., 2013; Murat and Balasubramanian, 2014; Rodriguez et al., 2012). Notably, binding of small molecules and/or ligands to the G4 structures can activate an R-loop-dependent DNA damage response, which will ultimately lead to different cellular consequences commensurate with the concentration and chemical nature of the ligands as well as their binding mode and selectivity for specific G4 motifs (Hampel et al., 2013; Hu et al., 2019; Paul et al., 2020; Amato et al., 2018).

In this study, we provide direct evidences of Hx and heme functions in the tumor microenvironment using *in vivo* prostate cancer murine models in $Hx^{-/-}$ mice as well as a large cohort of human cancer biopsies and plasma samples. Our findings demonstrate a previously unknown role and mechanism for labile heme in cancer growth and metastatic progression via G4:heme interaction and regulation of key G4-driven oncogenes thus suggest potential innovative therapeutic targets for cancer treatment.

RESULTS

Plasma Levels of Heme and Hx in Patients with PCa: Hx Associates with Clinical Outcome

To investigate whether retention of labile heme in the circulation and tumor microenvironment could be a marker for cancer progression, we measured the plasma levels of heme and Hx in a set of 26 patients with prostate cancer (PCa) and 7 healthy volunteers. We detected significantly higher levels of labile heme (Figure 1A) and lower levels of its scavenger Hx (Figure 1B) in the plasma of patients with cancer (low- or high-grade tumors) compared with healthy controls. Second, we validated the relevance of these findings in a larger cohort of PCa, including malignant and benign prostatectomy specimens from 341 patients (Mulvaney et al., 2016) and analyzed Hx expression in a tissue microarray (TMA) by immunohistochemistry. The Hx staining in the stroma was significantly weaker in moderately (Gleason score [GS] ≤ 7) and poorly differentiated (GS > 7) tumors as compared with benign tissues (Figures 1C and 1D), similar to what we observed in the plasma samples (Figure 1B).

Next, we assessed whether Hx in the tumor stroma could be used as predictive marker for cancer progression. Remarkably, low Hx levels in the stroma correlated with poor prognosis and earlier disease relapse based on the rising prostate-specific antigen (PSA) levels (biochemical recurrence [BCR]) (Figure 1E), whereas no major differences in the Kaplan-Meier progression-free survival curves based on the levels of Hx in cancer epithelial cells or stroma from benign tissues was observed (Figures 1F, S1A, and S1B). Interestingly, high Hx levels (based on the median H score cutoff) in the benign epithelium correlated with a better prognosis (Figure S1A).

Because labile heme is derived in large part from hemoglobin, we evaluated whether hemoglobin and Hx mRNA expression is altered in metastases of PCa. Interestingly, we found higher levels of hemoglobin subunit alpha 2 (HBA2) and Hx in metastatic tumors (Figures S1C and S1D) from the same Geo-profile-sample set previously used to show upregulation of heme oxygenase-1 (HO-1, encoded by *Hmox1)* expression in metastatic PCa (Nemeth et al., 2015).

Heme Increases Metastatic Outgrowth of Cancer

To assess whether changes of labile heme could promote tumor growth and progression in a mouse model *in vivo*, we injected PC3 cells subcutaneously in immuno-compromised animals, and we treated established tumors with Fe (III) heme (35 mg/kg, intraperitoneally [i.p.] daily, for 2 weeks) (hemin; referred as "heme" in prior research [Hedblom et al., 2019; Larsen et al., 2010] and throughout the text here for consistency) daily for the following 2 weeks. This dose of heme neither affected body weight nor survival of mice (data not shown). In agreement with previously published results using the same *in vivo* model but less frequent and slightly lower doses of heme (Leonardi et al., 2019), we did not observe a significant difference in the overall tumor volume in mice treated with heme compared with untreated mice (Figure S2A). However, we showed increased local invasion (Figure 2A) and detected higher numbers of lymph node (LN) metastases after heme treatment (Figure 2B). Consistently, the significant proliferation of cancerous cells in the tumor
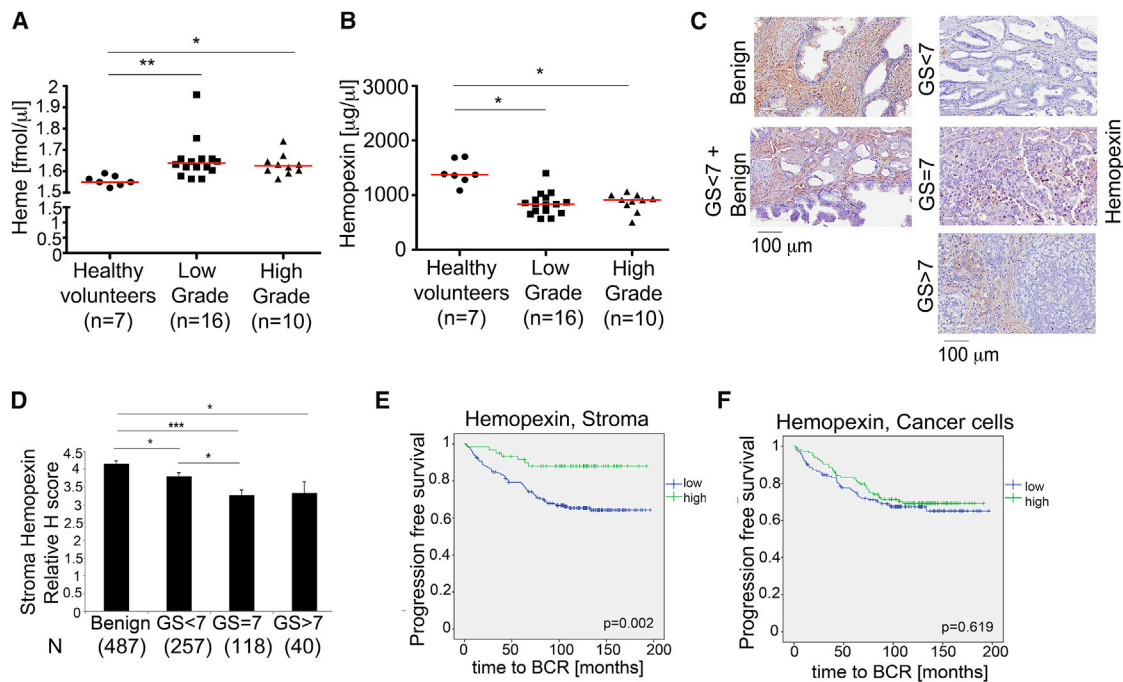
Figure 1. Hx Levels Correlate with a Better Outcome for Patients with PCa

(A and B) Measurements of heme and Hx levels in plasma samples obtained from patients with PCa. Low grade, patients with Gleason scores (GSs) of 6 or 7; high grade, patients with GSs of 8 or higher; healthy volunteers, donors with unknown cancer diagnoses. Scatter plot represents each measurments and median. ANOVA, *p < 0.05, **p < 0.01.

(C) Representative staining with an antibody against Hx in benign and cancer (well-differentiated, GSs < 7; moderately differentiated, GS = 7; poorly differentiated, GS > 7) tissues from 341 patients with PCa using tissue microarrays (TMAs). Scale bar 100 μm.

(D) Relative H score (= *Intensity × Percentage of positive cells*) of stromal Hx staining in the 341 patients with PCa and corresponding benign tissues. Number of cores used for each group is shown. Bar chart represents mean ± SEM. ANOVA, *p < 0.05, ***p < 0.001.

(E and F) Progression-free survival curves based on the BCR are shown in a follow-up for 200 months from initial prostatectomy. H scores for Hx in stroma (E) and in cancer cells (F) were analyzed with the median value as a cutoff for the survival analysis. Hazard ratio (95% confidence interval [95% CI]) for (E), 3.25 (1.50–7.08), **p = 0.002. Hazard ratio (95% CI) for (F), 1.13 (0.71–1.79), p = 0.619.

periphery upon heme treatment (Figures 2C and 2D) was accompanied by an upregulation of c-Myc, increased levels of Rb phosphorylation, and heme oxygenase-1 (HO-1) expression (Figure 2D). No changes in the expression levels of total Rb or HO-2 were detected (Figure 2D). Importantly, the increase of *c-MYC* at the mRNA levels suggested increased gene transcription (Figure S2B). We did not observe a difference in *Hmox1* mRNA expression levels in the mouse stroma cells (Figure S2C), suggesting that HO-1 is induced by heme primarily in cancer cells in the tumor microenvironment (Figure 2D).

To validate our findings in a clinically more relevant model, we implanted transgenic adenocarcinoma of the mouse prostate (TRAMP-C1; murine PCa cells) orthotopically into immunocompetent C57Bl6 mice (Figures 2E–2M) and treated those mice bearing established tumors in the prostate with heme. We observed enlarged tumors and increased numbers of LN metastases in mice treated with heme compared with control mice (Figure 2E–2H). Ki67 levels in both tumors and LN metastases were significantly higher in mice treated with heme than they were in control mice (Figures 2H and 2I). Further, tumors of animals treated with heme expressed higher levels of *c-MYC* and markers of invasion, such as matrix metalloproteinase-2

(*MMP2*) and −9 (*MMP9*) and urokinase-type plasminogen activator (*uPA*) (Figures 2J–2M).

Heme Sequestration by Hx in the Tumor Niche Blocks Aggressive Cancer Phenotype *In Vivo*

To assess the role of Hx in heme sequestration and in modulation of tumor growth, we used *Hx* knockout mice (*Hx*$^{−/−}$) in the orthotopic prostate models described above (Figure 2E). We reasoned that if heme is not scavenged by Hx in the tumor stroma or plasma via heme:Hx:CD91 receptor complexes, it should become directly available for cancer cells via cell membranes and/or heme transporters. PCa cells possess multiple known heme transporters, including *Abcg2*, *Flvcr1*, and *Hrg1*, which are all highly expressed relative to *CD91* or *Flvcr2* (data not shown). TRAMP-C1 cells implanted orthotopically into the prostate developed bigger tumors in *Hx*$^{−/−}$ mice compared with *Hx*$^{+/+}$ mice (Figure 2E). Further, *Hx*$^{−/−}$ mice with established TRAMP-C1 tumors and treated with heme developed significantly larger tumors and more LN metastases compared with untreated mice (Figures 2E–2I). Of note, increased expression levels of *c-MYC* and markers of invasion (*MMP9*, *MMP2*, and *uPA*) in *Hx*$^{−/−}$ tumors were observed upon heme treatment (Figures 2J–2M).
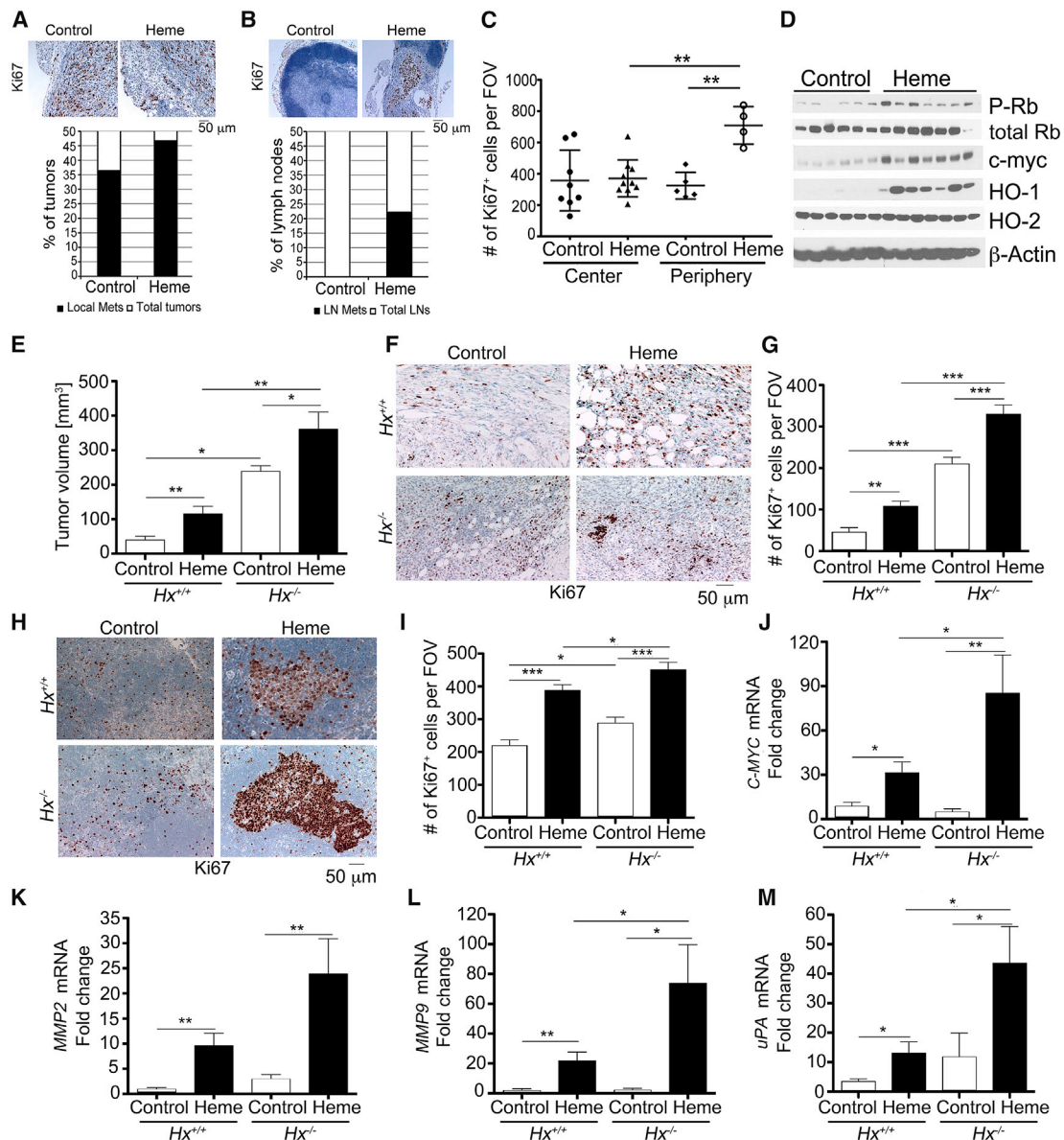
Figure 2. Role of Heme and Heme-Associated Proteins in Cancer Progression *In Vivo*

(A–C) PC3 xenografts were established in *nu/nu* mice for 2 weeks, and animals were treated with heme (35 mg/kg, i.p., daily) for the following 2 weeks. n = 3 mice/group with two tumors/mouse. Representative images and number of Ki67-positive cells infiltrating the local tumor stroma (A) or the LN (B) evaluated as a percentage of the control (n = 8–12 LNs/group). Scale bar 50 μm. Quantification of Ki67-positive cells is shown in (C). Scatter plot represents mean ± SEM. ANOVA, **p < 0.01.

(D) Immunoblot analysis of tumor lysates from PC3 xenografts as in (A)–(C).

(E) TRAMP-C1 tumors were established in $Hx^{+/+}$ and $Hx^{-/-}$ mice for 1 week, and animals were treated with heme (35 mg/kg, i.p., daily) for the following 4 weeks. Tumor size was measured with caliper at the time of sacrifice. n = 8 ($Hx^{+/+}$, control), n = 15 ($Hx^{+/+}$, heme), n = 5 ($Hx^{-/-}$, control), n = 8 ($Hx^{-/-}$, heme). ANOVA, *p < 0.05, **p < 0.01.

(F and G) Representative images (F) and number of Ki67-positive cells (G) infiltrating the local tumor stroma evaluated as number of stained cells per field of view (FOV). Scale bar 50 μm. ANOVA, **p < 0.01, ***p < 0.001.

(H and I) Representative images (H) and number of Ki67-positive cells (I) infiltrating the LNs evaluated as the number of stained cells per FOV. Scale bar 50 μm. Bar charts represent mean ± SEM. ANOVA, *p < 0.05, ***p < 0.001.

(J–M) qPCR analyses of *c-MYC* (J), *MMP-2* (K), *MMP-9* (L), and *uPA* (M) in TRAMP-C1 tumors established in $Hx^{+/+}$ and $Hx^{-/-}$ mice and treated as described above. Bar charts represent mean ± SEM. ANOVA, *p < 0.05, **p < 0.01, ***p < 0.001.
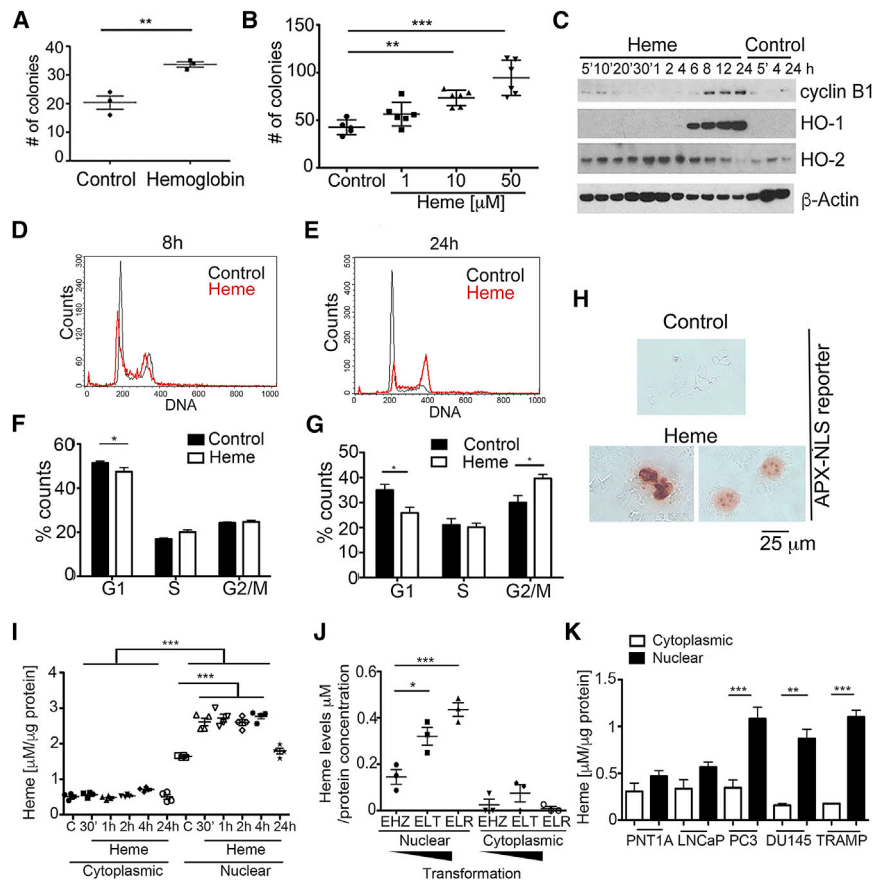
Figure 3. Heme Accelerates Tumor Growth and Accumulates in the Nucleus of Cancer Cells

(A) Anchorage-independent growth in soft agar of PC3 cells treated with hemoglobin (10 μM) for 3 weeks. Scatter plot represents mean ± SEM. n = 3 experiments performed in triplicate. Student's t test, **p < 0.01.

(B) Anchorage-independent growth in soft agar of PC3 cells treated with heme (1–50 μM) for 3 weeks. Scatter plot represents mean ± SEM. n = 4–5 experiments performed in triplicate. ANOVA, **p < 0.01, ***p < 0.001.

(C) Immunoblot analysis of cyclin B1, HO-1, and HO-2 levels in PC3 cells treated with heme (50 μM) over a 24-h time course. n = 4–5 independent experiments.

(D–G) Cell cycle analysis of PC3 cells treated with heme (50 μM) for 8 h and 24 h. Representative graphs are shown in (D) and (E), and quantifications are presented in (F) and (G). Bar charts represent mean ± SEM. n = 3 independent experiments performed in duplicate. ANOVA, *p < 0.05.

(H) Representative images of the nuclear heme measured by the nuclear heme sensor (ascorbate peroxidase containing a nuclear localization signal [APX-NLS]) in PC3 cells treated with heme (50 μM) for 24 h. Two examples of cells (strongly and medium positive) with APX-NLS staining are shown. Scale bar 25 μm. n = 3 independent experiments.

(I) Detection of heme levels in the subcellular fractions of PC3 cells at 30 min and 1, 2, 4, and 24 h after addition of exogenous heme. Scatter plot represents mean ± SEM. n = 3 independent experiments. ANOVA, ***p < 0.001.

(J) Detection of heme basal levels in the subcellular fractions of BJ fibroblasts (EHZ, ELT, and ELR) as measured by benzidine staining. Scatter plot represents mean ± SEM. n = 3 independent experiments. ANOVA, *p < 0.05, ***p < 0.001.

(K) Detection of heme basal levels in subcellular nuclear and cytoplasmic fractionations of PNT1A, LNCaP, PC3, DU145, and TRAMP-C1 cells. n = 3 independent experiments performed in triplicate. Bar charts represent mean ± SEM. Student's t test, **p < 0.01, ***p < 0.001.

To expand our understanding of the role of heme and Hx across multiple tumor types, we tested a similar approach using a lung cancer model (Figures S2D–S2F). In response to heme treatment, mice bearing subcutaneously implanted murine Lewis lung carcinoma (LLC) tumors showed increases in Ki67 staining at the edge of the tumor with invasive behavior (Figures S2E and S2F). Consistently, LLC cells inoculated into $Hx^{-/-}$ mice also displayed an invasive behavior at the edge of the tumors (Figures S2E and S2F). The increase in c-Myc levels was accompanied by both elevated total and phosphorylated Rb in LLC tumors (Figure S2D).

Heme Promotes Growth of Colonies in Soft Agar and Affects Cell Cycle

Because both hemoglobin and Hx are associated with more aggressive phenotypes, we evaluated whether heme derived from hemoglobin could similarly affect the growth of the human prostatic carcinoma cell line. Hemoglobin promoted colony growth of PC3 in soft agar *in vitro* (Figure 3A); similarly, heme treatment of PC3 cancer cells led to larger and more-numerous colonies in soft agar in a dose-dependent manner (Figures 3B

and S3A). Moreover, addition of heme to cancer cells activated cell-cycle-related pathways by inducing cyclin B1 and HO-1 expression levels (Figure 3C) and promoting the transition of PC3 cells through the G1-S and G2-M cell cycle phases (Figures 3D–3G, S3B, and S3C). In the presence of labile heme, fewer cells accumulated in the G1 phase at 8, 24, and 48 h, whereas the number of cells in G2/M phases was significantly higher at 24 and 48 h (Figures 3D–3G, S3B, and S3C), suggesting proliferative advantage in response to heme.

Labile Heme Accumulates in the Nucleus of Cancer Cells

Because we observed a strong induction of cell-cycle regulatory molecules by heme, we measured the intracellular heme levels. Using a nuclear-targeted heme sensor (Yuan et al., 2016) (Figure 3H) and colorimetric measurements (Figure 3I), we demonstrated the uptake and accumulation of heme in the nucleus upon treatment with exogenous heme in PC3 cells or fibroblasts (Figures 3I, S3D, and S3E). Nuclear heme levels were increased upon the addition of exogenous heme, reaching a plateau levels at 2–4 h after treatment of PC3 cells and returning to the baseline

after 24 h presumably because of increased activity of HO-1 (Figures 3I and 3C). The successful fractionations and HO-1 induction in the samples were confirmed (Figures S4A–S4D). We then assessed the basal levels of labile heme in the nuclear and cytoplasmic compartments of several normal (BE [human bronchial epithelial cells] and PNT1A [normal human prostate epithelium]) and cancer cell lines: PCa (LNCaP, DU145, PC3, and TRAMP-C1), lung cancer (A549 and LLC), as well as in the transformed BJ fibroblasts (Figures 3J–3K and S3E). Interestingly, basal labile heme levels were markedly higher in the nuclear fractions of cancer cell lines compared with normal epithelial cells (Figures 3K and S3E). Remarkably, the basal level of heme accumulation in the nucleus of fibroblasts was proportional to the degree of cellular transformation determined by the number of oncogenes introduced into the BJ fibroblasts (EHZ [hTERT], ELT [hTERT, large T antigen], and ELR [hTERT, large and small T antigen, HRas]) (Boehm et al., 2005) (Figure 3J). Moreover, the accumulation of nuclear labile heme levels was more pronounced in metastatic cancer cells (Figure 3K), indicating a possible correlation between nuclear labile heme and aggressiveness.

Heme Modulates a Subset of Genes Related to Cell Cycle and Cancer Progression

Because heme accumulates in the nuclear compartment in cancer cell lines, we asked whether heme could affect gene expression. We performed RNA sequencing (RNA-seq) analysis on PC3 cells treated with heme. To analyze the effect of heme on gene expression, we decided to collect cells at early time points (2 and 4 h upon treatment with heme), when the expression of HO-1 protein is still not detectable and thus the levels of heme are higher (Figures 3C and 3I). As expected, the top genes induced or repressed by heme after 4 h treatment were *Hmox1* and 5′-aminolevulinate synthase 1 (*ALAS1*), which are both key enzymes involved in the degradation or *de novo* synthesis of heme, respectively (Table S1). *Hmox1* mRNA was upregulated as early as 2 h after treatment and remained elevated at 4 h (Figure 4A); however, the protein was not detectable before 4 to 6 h after heme treatment (Figure 3C). In our RNA-seq analysis, *ALAS1* expression was initially upregulated at 2 h (~6-fold) and then suppressed by heme at 4 h as a negative feedback loop (Furuyama et al., 2007) (Tables S1 and S2). Consistent with our other findings (Figures 3C–3G), heme treatment significantly perturbed genes involved in cell-cycle progression leading to downregulation of *CCNE1*, *CCNA2*, *CCNE2*, *E2F2*, and *TGFB3* or upregulation of others, i.e., *CCNA1*, *MYC*, and *CDKN1A* at 2 h (Figure 4A). Similarly, genes associated with cell-cycle checkpoint, estrogen-mediated S-phase entry and cancer metastases (WNT, transforming growth factor beta [TGF-β], and MAPK/Erk1/2 pathways) were also altered by the addition of heme as assessed by pathway analysis (Figures 4B–4D). Importantly, gene enrichment analysis showed early induction of Ap-1 pathway genes, such as *c-MYC*, *FOSB*, *MMP9*, or *ERG1* (Figures 4E and 4F) and reduction of genes associated with rRNA processing (*UTP15*, *DKC1*, and *UTP6*). The top genes altered by heme are included in Figures 4E and 4F. The pattern of gene enrichment in response to heme was reversed after 4 h (Figure 4F).

By performing real-time PCR (Figures 4G–4P), we confirmed that *Hmox1* was strongly induced by heme in PC3 cells at 2 and 4 h (Figure 4G), and it was highly elevated in the tumors implanted into $Hx^{+/+}$ or $Hx^{-/-}$ mice and treated with heme (Figure 4I). *ALAS1* mRNA was induced by heme in PC3 cells after 2 h, but its expression returned to the baseline levels at 4 h after heme treatment (Figure 4H). There was no significant effect of heme on *ALAS1* mRNA in tumors *in vivo* (Figure 4M). A similar mRNA pattern of gene-expression change to *Hmox1* was detected for the zinc finger 469 (*ZNF469*) gene (Figures 4I and 4N). Furthermore, heme treatment led to higher and transient expression of genes controlling autophagy and metastases, *AMIGO2* (amphoterin-induced gene and open reading frame 2), and *ULK1* (Unc-51 like autophagy activating kinase 1) in PC3 cells after 2 h (Figures 4J and 4K). Those genes were also elevated in tumors isolated from mice treated with heme on the wild-type and $Hx^{-/-}$ background (Figures 4O and 4P).

Heme Induces c-MYC-Dependent uPA Expression

To assess the contribution of one of the top heme-regulated genes, c-MYC, in heme-mediated cellular effects, we stably transduced PC3 cells with short hairpin (sh) RNAs targeting *c-MYC* and achieved ~50% knockdown of the mRNA (Figure 5A) and protein (Figure 5B) suppressing heme-induced *c-MYC* expression without affecting their survival. Although induction of both *MMP2* and *uPA* was observed in control non-targeting shRNA PC3 cell upon heme treatment, only uPA displayed a *c-MYC*-dependent expression (Figures 5C and 5D). Indeed, knockdown of *c-MYC* blocked basal and heme-induced *uPA* levels (Figure 5D). Importantly, shRNA-mediated *c-MYC* downregulation was able to limit the heme-induced colony growth (Figure 5E).

More than 75% of *c-MYC* transcriptional activity is controlled by G4 sequences embedded in the gene promoter (Siddiqui-Jain et al., 2002). Interestingly, we found that the effect of heme on colony growth was blocked in cells concurrently treated with the well-established *c-MYC* G4 stabilizing molecule, GQC-05 (Figure 5F), suggesting the requirements of *c-MYC* expression for heme-induced cancer growth. Notably, GQC-05 completely suppressed *c-MYC* expression (Figure 5G), in striking contrast to heme (Figure 5G), but at the dose of 10 μM used in this study did not affect cell survival/growth as measured by crystal violet staining (Figure 5H). Consistently, GQC-05 strongly inhibited c-myc protein expression in a dose-dependent manner (Brown et al., 2011), whereas no changes in vascular endothelial growth factor (VEGF) levels were observed (Figure 5G). On the contrary, heme treatment was associated with increased c-myc protein expression (Figure 5G).

These findings indicate that heme promotes *uPA* expression in a *c-MYC*-dependent manner and demonstrate a heme-mediated control of *c-MYC* expression, potentially by altering *c-MYC* G4 structures stability (Figure 5G).

Heme:G4 Complexes Regulate Cancer Growth

Heme is able to stabilize the G4-containing sequence (also known as Pu27) within the *c-MYC* promoter (Siddiqui-Jain et al., 2002) (Figures 5I and 5J). We detected little changes in
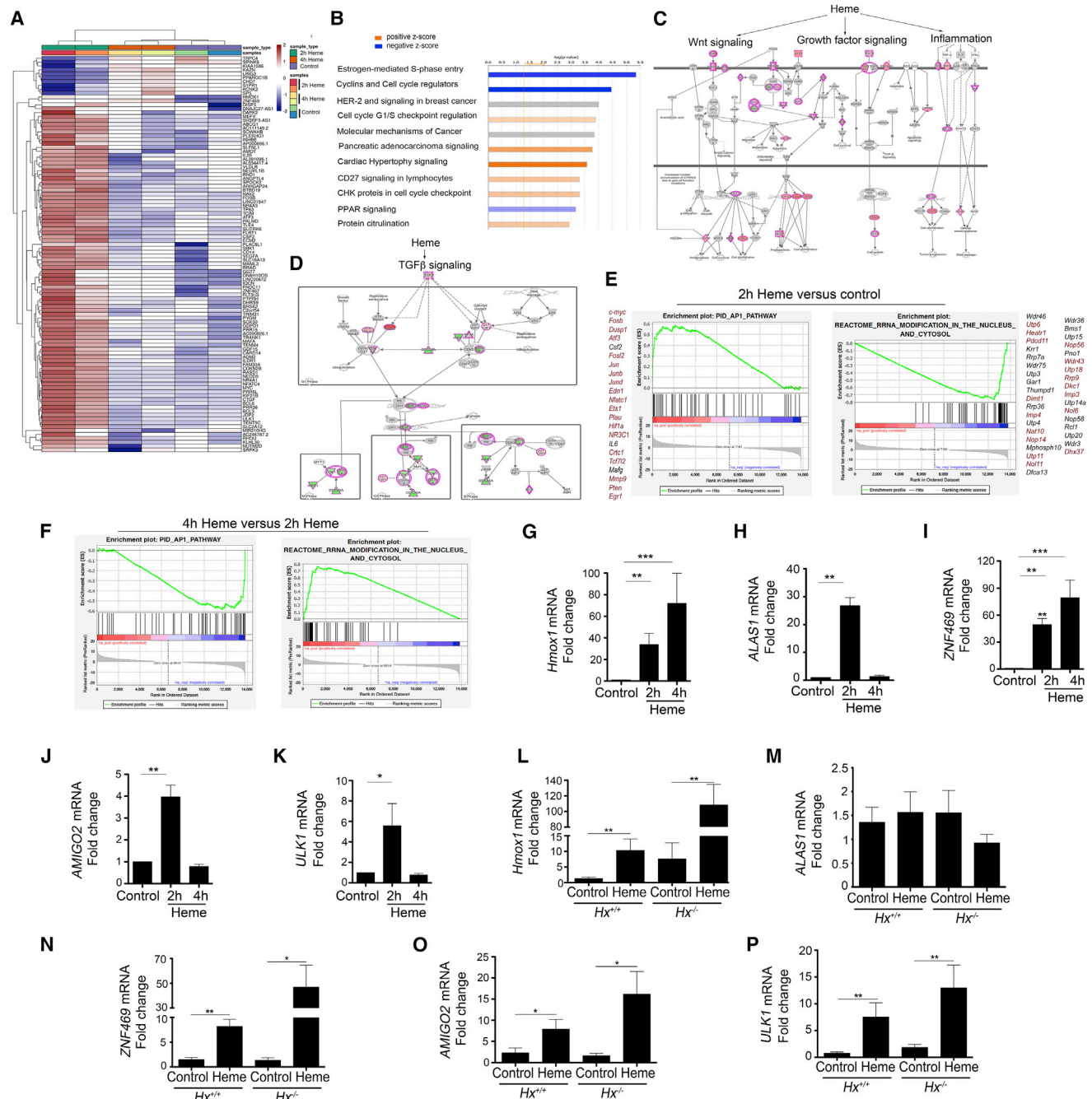
Figure 4. Heme Induces Selective Genes Controlling Metastases and Cell Cycle Progression

(A–F) Analysis of RNA-seq data from PC3 cells treated with heme (50 μM) for 2 h or 4 h and control cells. Heatmap is shown in (A). n = 2 per group. (B)–(D) Pathway analysis of the gene expression profiles as in (A). (E and F) Gene set enrichment analysis based on the functional annotation of the differentially expressed genes identified two key pathways: AP-1 and rRNA modification pathways in response to heme. The genes enriched within the pathways are labeled in red if they contain G4 in their regulatory elements.

(G–K) qPCR analysis of *Hmox1 (HO-1)* (G), *ALAS1* (H), *ZNF469* (I), *AMIGO2* (J), and *ULK1* (K) in PC3 cells treated with heme (50 μM) for 2 h or 4 h. Bar charts represent mean ± SEM. ANOVA, *p < 0.05, **p < 0.01, ***p < 0.001.

(L–P) qPCR analysis of *Hmox1 (HO-1)* (L), *ALAS1* (M), *ZNF469* (N), *AMIGO2* (O), and *ULK1* (P) in TRAMP-C1 tumors established in $Hx^{+/+}$ and $Hx^{-/-}$ mice and treated with heme as above. Bar charts represent mean ± SEM. ANOVA, *p < 0.05, **p < 0.01.
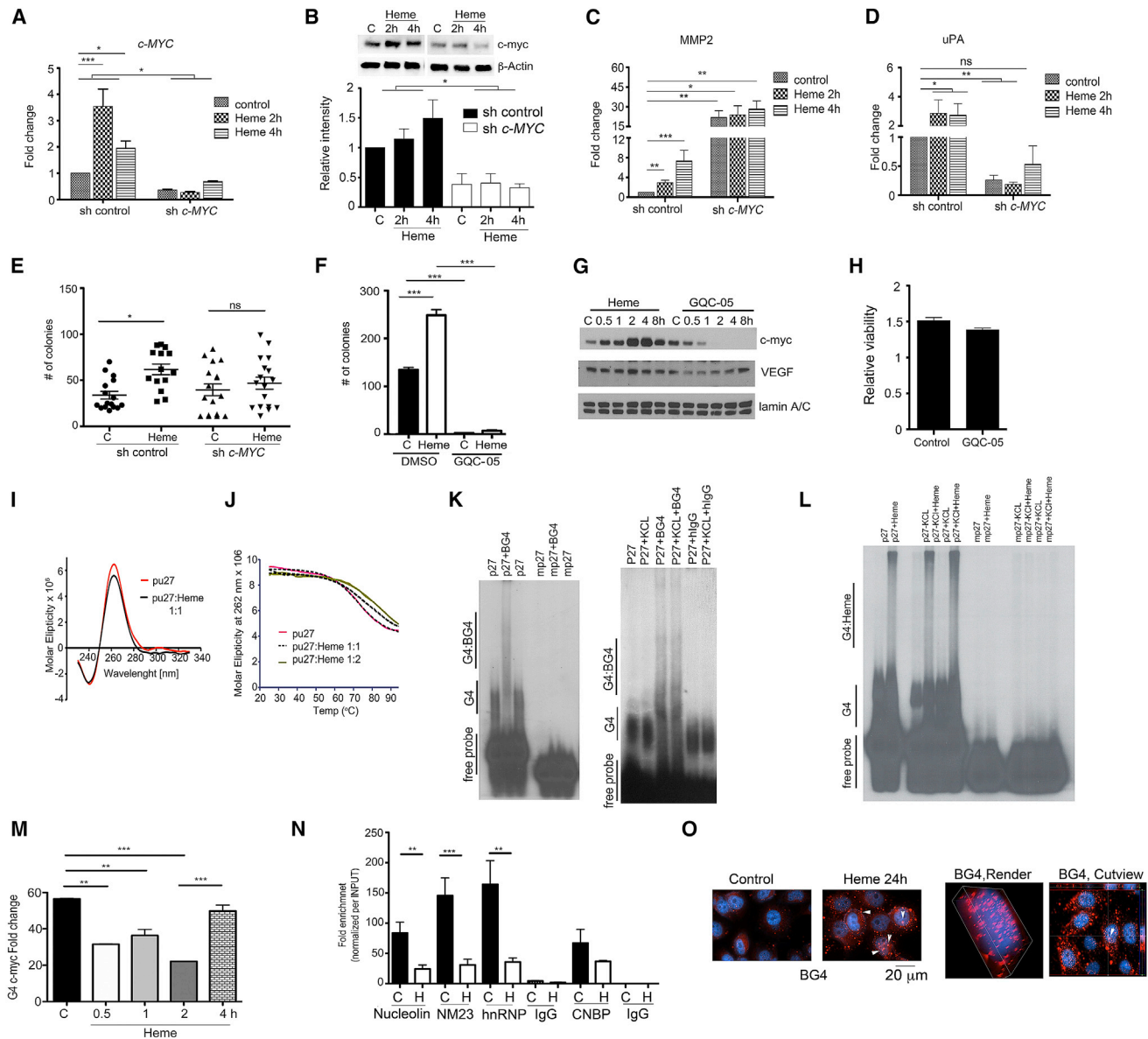
Figure 5. Heme Activates *c-MYC* Expression in Part via Binding to DNA G4 Structure in Its Promoter

(A and B) qPCR (A) and western blot (B) analysis of c-MYC in PC3-sh-control and PC3-sh-c-*myc* cells treated with heme (50 μM) for 2 h or 4 h. Bar charts represent mean ± SEM. ANOVA, *p < 0.05, ***p < 0.001.

(C and D) qPCR analysis of *MMP2* (C) and *uPA* (D) in PC3-sh-control and PC3-sh-c-*myc* cells treated with heme (50 μM) for 2 h or 4 h. Bar charts represent mean ± SEM. ANOVA: *p < 0.05, **p < 0.01, ***p < 0.001.

(E) Anchorage-independent growth in soft agar of PC3-sh-control and PC3-sh-c-*myc* treated with heme (50 μM) for 3 weeks. Scatter plot represents mean ± SEM. n = 3 independent experiments. ANOVA, *p < 0.05. n.s., not significant.

(F) Anchorage-independent growth in soft agar of PC3 cells cultured in the presence or absence of GQC-05 (10 μM) or vehicle (DMSO) with or without heme (50 μM) for 3 weeks. Bar chart represents mean ± SEM. n = 3 experiments performed in triplicate. ANOVA, ***p < 0.001.

(G) Western blot analysis of c-*myc*, VEGF, and lamin A/C in cell lysates from PC3 cells treated with heme (50 μM) or GQC-05 (10 μM) for 0.5–8 h. A representative blot of three independent experiments is shown.

(H) Crystal violet staining of PC3 cells treated for 48 h with GQC-05 (10 μM). Bar chart represents mean ± SEM. n = 3 independent experiments.

(I) CD spectra with 1:1 heme:Pu27 ratio demonstrating molecular ellipticity at 262 nm. The peak is maintained upon addition of heme, indicating a parallel G4 structure.

(J) Melting temperature of the heme:Pu27 complexes evaluated at 262 nm by CD. Melting temperature for pu27 oligonucleotide was 72.36°C, for Pu27:heme, 1:1 was 78.27°C, and for Pu27:heme, 1:2 was 84.15°C.

(K) EMSA was performed using the wild-type G4-Pu27 (p27) or the mutated G4-Pu27 (mp27) sequence found in the *c-MYC* promoter region in the presence of an antibody against G4 (BG4). Results are representative of three experiments.

(legend continued on next page)

the circular dichroism (CD) spectrum upon addition of heme, supporting the idea that G4 structures are likely being maintained or slightly distorted, as confirmed by a measurement of the melting temperature upon the addition of heme to G4 DNA sequence *in vitro* (Figure 5J).

To address the heme:G4 interaction, we used an anti-G4 antibody (the BG4 immunoglobulin G [IgG]) that recognizes G4 structures (Biffi et al., 2014b) and IgG control. We observed specific binding between the BG4 antibody and the Pu27 *c-MYC* promoter sequence forming G4 structures (Figure 5K), whereas no binding occurred between Pu27 *c-MYC* and IgG control (Figure 5K). Such complexes were lost when a mutated Pu27 (pu27-M) sequence, which is unable to form G4 *in vitro*, was used (Figure 5K). These results led us to test whether heme could complex directly with G4 structures (Figure 5L). A strong interaction between heme and G4 was confirmed with the Pu27 *c-MYC* promoter sequence as a model (Figure 5L). Chromatin immunoprecipitation (ChIP) with anti-BG4 antibody in the PC3 cells showed suppression of G4 structures in the *c-MYC* promoter 0.5–2 h after heme treatment and enrichment to baseline levels at 4 h (Figure 5M). The G-quadruplex recognition, stabilization, and unwinding at Pu27 is controlled by four major proteins: (1) nucleolin (involved in the formation and stabilization of G4 in *c-MYC* promoter [González et al., 2009]), (2) non-metastatic 23-H2 (NM23-H2, a transactivator of *c-MYC*) (Berberich and Postel, 1995), (3) cellular nucleic-acid-binding protein (CNBP, an activator of parallel G4 structure) (Borgognone et al., 2010; Chen et al., 2013; Michelotti et al., 1995), and (4) heterogenous nuclear ribonucleoprotein K (hnRNPK, an activator of *c-MYC* expression by binding to single-stranded DNA) (Tomonaga and Levens, 1995). Therefore, we examined by ChIP whether recruitment of these four factors to the G4-rich region of *c-MYC* promoter was impaired in PC3 cells treated with heme. We confirmed the effective immunoprecipitation with the specific antibodies by western blot (Figures S5A and 5B). We detected CNBP and NM23-H2 in immunoprecipitates from control or heme-treated cells with anti-CNBP or anti-NM23-H2 antibodies, respectively (Figure S5A). We also confirmed the same efficiency of pull-down with antibodies against hnRNPK and nucleolin in the ChIP samples (Figure S5B). We found that the interaction of all four proteins with the *c-MYC* promoter was hampered at 2 h after heme treatment (Figures 5N, S5A, and S5B) with the most significant decreased enrichment of NM23-H2. Interestingly, the enrichment of CNBP at Pu27 was only slightly but not significantly decreased in cells treated with heme compared with untreated cells (Figure 5N).

Immunofluorescence staining of heme-treated cells using the BG4 antibody revealed increased G4 content in both the nucleus and cytoplasm of PC3 cells at 24 h after treatment with heme (Figure 5O), which aligns with our findings of dynamic

changes in G4 content in response to heme. Because the pattern of G4 enrichment in the *c-MYC* promoter corresponded to the expression pattern of *c-MYC* observed by RNA-seq (low G4 at 2 h corresponds to high *c-MYC* expression and baseline G4 at 4 h to baseline level of *c-MYC* levels in heme-treated cells), we sought to determine whether the genes responsive to heme treatment detected by RNA-seq exhibited G4 regions in their promoter. Not surprisingly, as many as ∼60% of the top heme-regulated genes were enriched in G4 sequences (Figure 4E; Table S3).

Presence of G4 Structure Correlates Inversely with Patient Outcome

To assess the clinical significance of G4, we used the TMA of 341 patients with PCa as above (Figure 1) and analyzed nuclear staining of G4 in epithelial and stroma cells (Figures 6A and 6B). Advanced PCa biopsies were associated with low G4 levels (Figure 6C). Interestingly, low G4 levels correlated with poor prognosis and earlier relapse similarly to Hx (Figure 6D). Strikingly, three patients with BG4 score <1 displayed very poor prognosis (Figure 6E). No association with G4 levels was observed for the cancer stroma component and the stroma or epithelial benign counterparts (Figures S6A–S6C).

DISCUSSION

In this study, we addressed the question of whether high levels of labile heme could have a role in cancer progression and how alterations of its scavenger Hx might contribute to the aggressiveness of the tumor behavior (Figure 6F). The role of heme, beyond the function of heme present in the cores of proteins, either as co-factors or regulatory element (i.e., in hemoproteins), is poorly understood. Heme is part of several nuclear transcription factors, including Rev-Erbα, NPAS2, Bach1, and Drosha (Burris, 2008; Carter et al., 2016; Dioum et al., 2002; Faller et al., 2007; Yin et al., 2007). Only recently, the identification of multiple heme transporters and the use of the heme sensors in the nucleus (Hanna et al., 2016; Yuan et al., 2016) have allowed monitoring of the trafficking of heme to the nucleus. In this study, we showed that heme accumulates in the nucleus of cancer cells and controls expression of key target genes, such as *c-MYC*, containing G4 structures in the promoters. Although previous work suggested that porphyrins interact with G4s and can affect G4 stability and function (Saito et al., 2012b), the *in vivo* relevance has never, to our knowledge, been investigated.

Repeated exposures of normal or cancer cells to heme may occur during hemolysis or cell death as well as upon administration of heme-arginate, a compound used to treat porphyrias. Severe hemolysis and premature death in mice lacking the peroxiredoxin-1 (*Prdx1*) gene correlate with higher incidence of

(L) EMSA was performed using p27 and mp27 G4 sequences incubated for 20 min with 50 μM heme before loading in the presence of the BG4 antibody. n = 3 independent experiments.

(M) ChIP analysis with anti-BG4 antibody in PC3 cells treated with heme (50 μM) for 0.5, 1, 2, and 4 h. n = 3–4 independent experiments performed in duplicate. Bar chart represents mean ± SEM. ANOVA, **p < 0.01, ***p < 0.001.

(N) ChIP analyses with anti-nucleolin, anti-NM23-H2, anti-CNBP, and anti-hnRNPK antibodies in PC3 cells treated with heme (50 μM) for 2 h. n = 2 independent experiments performed in duplicates. Bar chart represents mean ± SEM. ANOVA, **p < 0.01, ***p < 0.001.

(O) Immunofluorescence staining for BG4 in PC3 cells treated with 50 μM heme for 24 h. Scale bar 20 μm. n = 3 independent experiments.
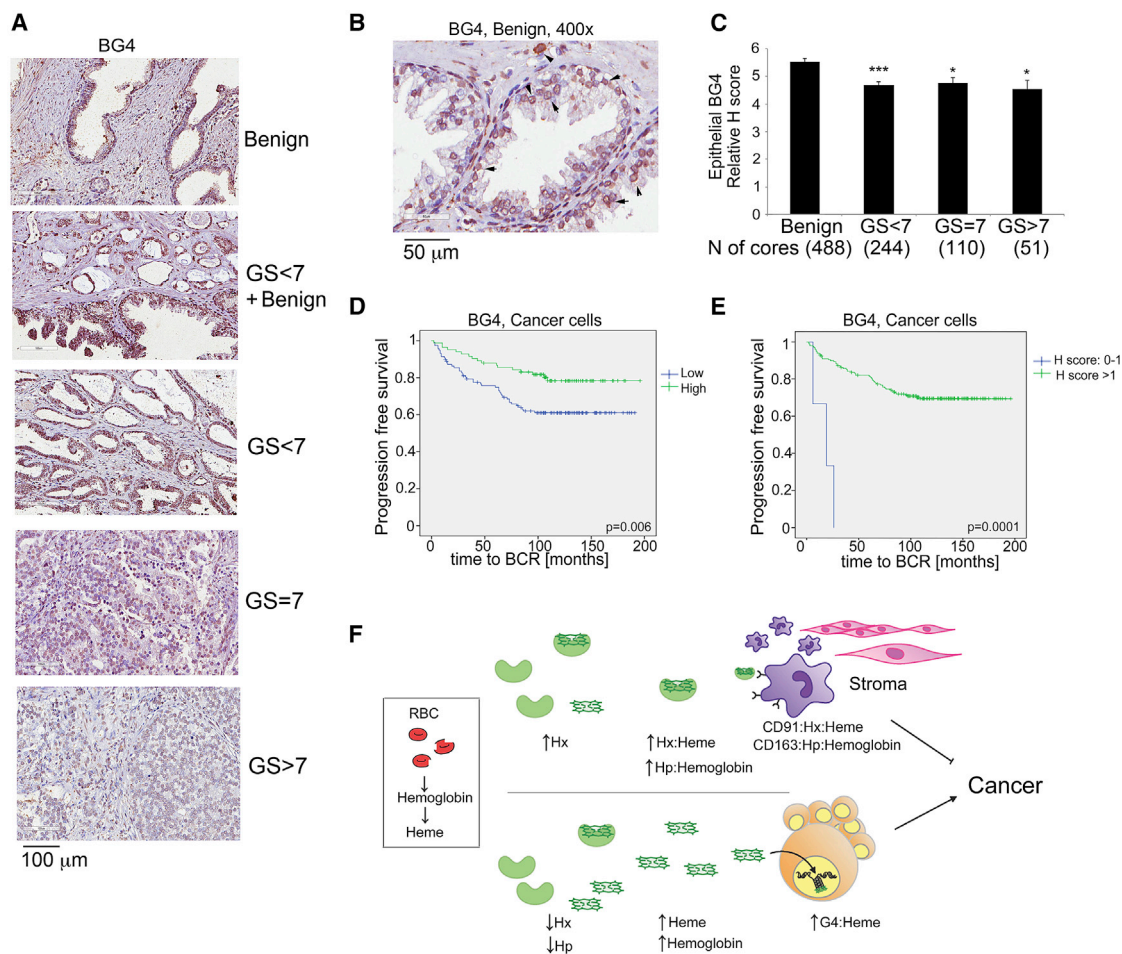
Figure 6. BG4 Levels Correlate with Cancer Progression and Progression-free Survival of Patients with Prostate Cancer
(A and B) Representative staining with an antibody against G4 in benign and cancer (well-differentiated, GS < 7; moderately differentiated GS = 7; or poorly differentiated, GS > 7) tissues from 341 patients with PCa as in Figure 1C. Scale bars 100 μm (A) and 50 μm (B).
(C) Relative H score (= *Intensity × Percentage of positive cells*) of BG4 staining as in Figure 1C. *p < 0.05, ***p < 0.001.
(D and E) Progression-free survival curves based on the BCR are shown in a follow-up for 200 months from initial prostatectomy. Bar chart represents mean ± SEM. H score for BG4 in cancer cells (D) was analyzed with the median value as a cutoff for the survival analysis. Hazard ratio (95% CI) for (D), 2.86 (1.38–5.91), p = 0.006. Hazard ratio (95% CI) for (E), 18.84 (5.11–69.39), p = 0.0001. Note: Three patients with negative H score for BG4 were compared with remaining patients with H score > 1 in (E) to emphasize the role of BG4 in cancer progression.
(F) Scheme illustrating the role of heme and heme-associated proteins in cancer progression. Hemoglobin and heme can be scavenged by Hp or Hx and taken up by macrophages via binding to CD169 or CD91, respectively. If Hx is not present, heme accumulates in the nucleus of cancer cells and binds to G4 DNA in the regulatory regions of specific genes to facilitate their expression and progression of cancer.

malignancies, such as sarcomas, lymphomas, and carcinomas (Neumann et al., 2003). Based on our findings, this phenotype could be ascribed to the heme-induced cancer cell colony growth and formation of metastases *in vivo*. Interestingly, several cases of hemolytic uremic syndrome have been described in advanced PCa patients (Mungall and Mathieson, 2002; Ramos et al., 2013). We established a strong predictive value of Hx levels in the stroma of a cohort of 341 patients with PCa and primary tumors. With plasma from a smaller cohort of patients (n = 26), we discovered an inverse correlation between heme and Hx levels. Remarkably, higher Hx levels in the stroma, with presumably lower labile heme levels in the tumor, are associated with a better survival of patients with PCa. A larger cohort of plasma

and urine samples should be tested to assess the role of heme as a PCa biomarker in the future. We propose that Hx binds labile heme with strong affinity allowing its uptake by LPR1/CD91-positive cells. LPR1/CD91 is expressed at low levels in the stroma of PCa according to the Human Atlas. Presence of Hx/CD91 in healthy tissues might be a mechanism that prevents entering of heme into pre-malignant or cancer cells and promoting their growth. Interestingly, we found that *mRNA* levels of *Hmox1*, *Hx*, and *HBA2* are highly expressed in metastatic samples of PCa. The increase in HBA2 could be associated with increase load of labile heme coming from erythrocytes as well as dying cancer cells or healthy cells (inflammatory cells) at the tumor niche. However, we have no direct evidence for the elevated

heme levels in the metastatic niche, and the levels of HBA2 or Hx *mRNA* obtained from Geo Profiles using metastatic samples do not directly suggest how much free versus protein-bound heme is present in the niche. Importantly, the biochemical responses to heme are different from that of heme:Hx complexes and range from activation of cell growth to apoptosis (Eskew et al., 1999) but are poorly understood. Prior work indicated that decreased Hx levels in patients with acute respiratory distress syndrome (ARDS) or burns and in premature infants may lead to insufficient clearance of heme and, therefore, administration of Hx may benefit those patients (Lin et al., 2015).

Metastatic phenotype of tumors exposed to labile heme in the absence of Hx indicates the essential role of this heme scavenger protein in tumor progression. We demonstrated an increased anchorage-independent growth of cancer cells in response to heme that correlates with changes in expression of cell cycle regulators and metastatic genes, such as *c-MYC* and metalloproteinases. Several other studies have reported the importance of MMPs in PCa cell proliferation, invasion, and metastasis (Quigley et al., 2018; Wegiel et al., 2008) (Wyganowska-Świątkowska et al., 2019). Of note, we found that heme-induced *c-MYC* levels control the expression of *uPA*, similar to hypoxia-induced *uPA* expression (Hou et al., 2007). Because of its role in the process of extracellular matrix degradation, uPA is a poor prognostic marker for PCa, and its expression levels have been associated with distant metastasis and tumor progression (Duffy, 2002; Nassir, 2020; Shariat et al., 2007). Previous studies, applying higher doses of heme (70 μM versus the 50 μM dose used in our study) and opposite of pharmacological kinetics (preconditioning with heme before injection of tumor cells and not after the tumor is established, as described herein), reported suppression of PCa cell migration/invasion, MMP9, and uPA expression upon heme treatment (Gueron et al., 2009; Jaworski et al., 2017), in contrast to our results. However, the reason for that apparent discrepancy is 2-fold. First, the higher doses of heme may be toxic to cancer cells, whereas the lower dose may be permissive for invasive growth; second, conditioning the mice before the tumor is established and not after, evaluates the effect of heme on the immune cell phenotype rather than in cancer progression.

c-MYC is a potent oncogene aberrantly expressed in approximately 80% of human malignancies (Dejure and Eilers, 2017). In PCa, c-MYC drives tumor proliferation and the expression of androgen receptor (AR) gene splice variants, and its levels are associated with biochemical recurrence after radical prostatectomy (Cui et al., 2020) (Bai et al., 2019; Hawksworth et al., 2010). However, knockdown of *c-MYC* in fibroblasts was associated with reduced levels of *c-MYC* in the prostate tumor stroma and led to increased PCa cell invasion (Valencia et al., 2014). Although these findings may indicate that c-myc could be a tumor suppressor in the cancer stroma, our data clearly show that heme-induced *c-MYC* promotes tumor growth. *c-MYC* expression is tightly controlled by the presence of G4 within the promoter (Siddiqui-Jain et al., 2002). The cationic porphyrin, TMPyP4 can bind to the G4 within *c-MYC* gene promoter thereby repressing its transcription (Siddiqui-Jain et al., 2002). Unlike TMPyP4, TMPyP2 binds less efficiently to the G4 within the *c-MYC* promoter. Although TMPyP4 and labile heme share

the same porphyrin ring structure and cationic center capable of binding G4 structures, our studies show that, in contrast to TMPyP4-mediated repression of transcription (Siddiqui-Jain et al., 2002), heme promotes *c-MYC* expression. Recent data show that the G4-stabilizing molecule GQC-05 efficiently increases the CD spectra peak at 262 nm, resulting in a decreased expression of *c-MYC* (Brown et al., 2011). We show that GQC-05 blocks heme-mediated colony growth, suggesting that heme may drive cancer colony formation specifically through *c-MYC* promoter engagement and that both molecules may compete with each other for binding to the G4 structures. We demonstrated that heme blunts the interaction between *c-MYC* promoter and G4-interacting proteins nucleolin, NM23-H2, and hnRNPK at the time when *c-MYC* mRNA expression peaks. The early and transient destabilization and unwinding of G4 complexes upon heme treatment (0.5–2 h) is associated with impaired binding of NM23-H2:G4 and a decreased interaction of hnRNPK and nucleolin with the pu27 promoter element at 2 h. The presence of CNBP was only slightly, but not significantly, reduced at the *c-MYC* promoter in response to heme. CNBP might contribute to stabilization of parallel G4 structure and enhanced *c-MYC* transcription (Borgognone et al., 2010; Chen et al., 2013). It was shown that CNBP promotes a transient reduction of *c-MYC* expression, which is later reversed by interaction by CNBP with NM23-H2 (Chen et al., 2013). However, CNBP was also reported to bind and stabilize the G4 in the promoter of hnRNPK, resulting in suppression of transcription (Qiu et al., 2014; Qiu et al., 2015). In contrast, CNBP promotes *K-ras* expression by unwinding the G4 structure (David et al., 2019). The dynamic changes in *c-MYC* promoter occupancy by those proteins and thus alterations of heme:G4 structures are likely responsible for the transient but robust induction of *c-MYC* expression in response to heme.

Sixty percent of the heme-targeted genes display G4-rich promoters supporting the hypothesis of heme direct binding to those structures. Our data show that key genes driving cell cycle (growth factor signaling, cyclins and cell cycle regulators of S-phase), epithelial to mesenchymal transition (EMT; TGF-β and Wnt pathways), and inflammation are transiently upregulated by heme before HO-1 protein induction, and many of them have been previously associated with increased invasiveness and metastases. Most G4-driven genes within the identified AP-1 and rRNA processing pathways return to the baseline 4 h after heme treatment, which might be due to accelerated entrance of PC3 cells into the S phase in the presence of heme. The highly dynamic changes in gene expression are likely due to a direct interaction of heme with DNA and transient destabilization of G4 structure in the promoters. In contrast to previous studies (Biffi et al., 2014b), but in accordance with the hypothesis that decreased G4 formation enables gene expression to be turned on, we demonstrated lower levels of G4 in the nucleus of patients with poor survival and advanced disease. A comprehensive analysis of disease progression was missing in the prior work. Interestingly, unlike Hx expression, the intensity of G4 structure staining in the stroma was not correlated with a clinical outcome. Likely, the heme:G4 quadruplex formation in healthy cells occurs at low frequency, given the limited ability of healthy cells to accumulate nuclear heme. By contrast, we showed that

cancer cells can tolerate accumulation of labile heme in the nucleus, which may explain the modulatory effect on G4 in the cancer compartment rather than in the stroma.

In summary, we uncovered the functional role of nuclear labile heme accumulation as a driver of metastasis via interaction with G4 structures embedded in the promoter regions of critical genes such as *c-MYC*. We described the antitumor function of Hx and connected scavenging of heme to patient outcome. Numerous implications that arise from this study include (1) the potential use of heme levels as a biomarker for patients with PCa, (2) the reclassification of heme (i.e., red meat or treatment with heme arginate) as a DNA intercalating agent able to turn on oncogene expression and metastatic gene expression profile via interaction with G4, and (3) the use of Hx and BG4 as clinical biomarkers associated with cancer dissemination in prostate malignancies.

STAR★METHODS

Detailed methods are provided in the online version of this paper and include the following:

- KEY RESOURCES TABLE
- RESOURCE AVAILABILITY
  - Lead Contact
  - Materials Availability
  - Data and Code Availability
- EXPERIMENTAL MODEL AND SUBJECT DETAILS
  - Cell lines
  - Patients samples
  - Animal models
- METHOD DETAILS
  - Reagents
  - Soft agar colony assay
  - Cell cycle analysis
  - Tumor models
  - BG4 antibody generation
  - IHC and immunostaining
  - Nuclear/Cytoplasmic Fractionation
  - Immunoblotting
  - Chromatin immunoprecipitation (ChIP):
  - RNA-sequencing
  - Oligonucleotides, EMSA and Circular Dichroism
  - Real time PCR
  - Viability assay
  - Geo Profiles
  - Heme and hemopexin measurement
- QUANTIFICATION AND STATISTICAL ANALYSIS
  - RNA-seq bioinformatics analyses
  - Differential Gene Expression, Pathway and Gene Set Enrichment Analysis
  - Statistics

SUPPLEMENTAL INFORMATION

Supplemental Information can be found online at https://doi.org/10.1016/j.celrep.2020.108181.

AUTHOR CONTRIBUTIONS

G.C., A.D.R., M.L., and B.W. designed the study. M.L. and B.W. conceived the original idea and acquired an original set of *in vitro* and *in vivo* data using PC3 xenograft models. A.D.R. performed electrophoretic mobility shift assay (EMSA) experiments. G.C. and B.W. performed *in vivo* experiments and analyses of TMA. S.U. did the ChIP assays. S.-Y.C. helped with the ChIP protocol. E.C. performed immunohistochemistry (IHC) and immunofluorescence (IF) staining. A.H. and R.C. performed colony assays with genetic quality control (GQC) and part of the western blots. A.K., M.P., and A.S. performed TMA staining and analyzed the data. L.H. and P.Z. performed CD experiments and provided reagents for the G4 study. M.A.B. analyzed the RNA-seq data. D.G.T. and A.E. provided input on c-myc regulation and EMSA. E.T. provided Hx knockout (KO) mice. M.L., G.C., A.D.R., and B.W. wrote the paper with input from all authors. B.W. supervised the work.

DECLARATION OF INTERESTS

The authors declare no competing interests.

REFERENCES

Amato, J., Pagano, A., Capasso, D., Di Gaetano, S., Giustiniano, M., Novellino, E., Randazzo, A., and Pagano, B. (2018). Targeting the BCL2 gene promoter G-quadruplex with a new class of furopyridazinone-based molecules. ChemMedChem *13*, 406–410.

Ambrus, A., Chen, D., Dai, J., Jones, R.A., and Yang, D. (2005). Solution structure of the biologically relevant G-quadruplex element in the human c-MYC promoter. implications for G-quadruplex stabilization. Biochemistry *44*, 2048–2058.

Bai, S., Cao, S., Jin, L., Kobelski, M., Schouest, B., Wang, X., Ungerleider, N., Baddoo, M., Zhang, W., Corey, E., et al. (2019). A positive role of c-Myc in regulating androgen receptor and its splice variants in prostate cancer. Oncogene *38*, 4977–4989.

Balasubramanian, S., Hurley, L.H., and Neidle, S. (2011). Targeting G-quadruplexes in gene promoters: a novel anticancer strategy? Nat. Rev. Drug Discov. *10*, 261–275.

Berberich, S.J., and Postel, E.H. (1995). PuF/NM23-H2/NDPK-B transactivates a human c-myc promoter-CAT gene via a functional nuclease hypersensitive element. Oncogene *10*, 2343–2347.

Biffi, G., Tannahill, D., McCafferty, J., and Balasubramanian, S. (2013). Quantitative visualization of DNA G-quadruplex structures in human cells. Nat. Chem. *5*, 182–186.

Biffi, G., Di Antonio, M., Tannahill, D., and Balasubramanian, S. (2014a). Visualization and selective chemical targeting of RNA G-quadruplex structures in the cytoplasm of human cells. Nat. Chem. *6*, 75–80.

Biffi, G., Tannahill, D., Miller, J., Howat, W.J., and Balasubramanian, S. (2014b). Elevated levels of G-quadruplex formation in human stomach and liver cancer tissues. PLoS ONE *9*, e102711.

Boehm, J.S., Hession, M.T., Bulmer, S.E., and Hahn, W.C. (2005). Transformation of human and murine fibroblasts without viral oncoproteins. Mol. Cell. Biol. *25*, 6464–6474.

Borgognone, M., Armas, P., and Calcaterra, N.B. (2010). Cellular nucleic-acid-binding protein, a transcriptional enhancer of c-Myc, promotes the formation of parallel G-quadruplexes. Biochem. J. *428*, 491–498.

Brooks, T.A., and Hurley, L.H. (2009). The role of supercoiling in transcriptional control of MYC and its importance in molecular therapeutics. Nat. Rev. Cancer *9*, 849–861.

Brooks, T.A., and Hurley, L.H. (2010). Targeting MYC Expression through G-quadruplexes. Genes Cancer *1*, 641–649.

Brooks, T.A., Kendrick, S., and Hurley, L. (2010). Making sense of G-quadruplex and i-motif functions in oncogene promoters. FEBS J. *277*, 3459–3469.

Brown, R.V., Danford, F.L., Gokhale, V., Hurley, L.H., and Brooks, T.A. (2011). Demonstration that drug-targeted down-regulation of MYC in non-Hodgkins lymphoma is directly mediated through the promoter G-quadruplex. J. Biol. Chem. *286*, 41018–41027.

Burris, T.P. (2008). Nuclear hormone receptors for heme: REV-ERBα and REV-ERBβ are ligand-regulated components of the mammalian clock. Mol. Endocrinol. *22*, 1509–1520.

Carter, E.L., Gupta, N., and Ragsdale, S.W. (2016). High affinity heme binding to a heme regulatory motif on the nuclear receptor Rev-erbβ leads to its degradation and indirectly regulates its interaction with nuclear receptor corepressor. J. Biol. Chem. *291*, 2196–2222.

Chandran, U.R., Ma, C., Dhir, R., Bisceglia, M., Lyons-Weiler, M., Liang, W., Michalopoulos, G., Becich, M., and Monzon, F.A. (2007). Gene expression profiles of prostate cancer reveal involvement of multiple molecular pathways in the metastatic process. BMC Cancer *7*, 64.

Chen, S., Su, L., Qiu, J., Xiao, N., Lin, J., Tan, J.H., Ou, T.M., Gu, L.Q., Huang, Z.S., and Li, D. (2013). Mechanistic studies for the role of cellular nucleic-acid-binding protein (CNBP) in regulation of c-myc transcription. Biochim. Biophys. Acta *1830*, 4769–4777.

Cui, S.Z., Lei, Z.Y., Guan, T.P., Fan, L.L., Li, Y.Q., Geng, X.Y., Fu, D.X., Jiang, H.W., and Xu, S.H. (2020). Targeting USP1-dependent KDM4A protein stability as a potential prostate cancer therapy. Cancer Sci. *111*, 1567–1581.

David, A.P., Pipier, A., Pascutti, F., Binolfi, A., Weiner, A.M.J., Challier, E., Heckel, S., Calsou, P., Gomez, D., Calcaterra, N.B., and Armas, P. (2019). CNBP controls transcription by unfolding DNA G-quadruplex structures. Nucleic Acids Res. *47*, 7901–7913.

Dejure, F.R., and Eilers, M. (2017). MYC and tumor metabolism: chicken and egg. EMBO J. *36*, 3409–3420.

Dioum, E.M., Rutter, J., Tuckerman, J.R., Gonzalez, G., Gilles-Gonzalez, M.A., and McKnight, S.L. (2002). NPAS2: a gas-responsive transcription factor. Science *298*, 2385–2387.

Drygin, D., Siddiqui-Jain, A., O'Brien, S., Schwaebe, M., Lin, A., Bliesath, J., Ho, C.B., Proffitt, C., Trent, K., Whitten, J.P., et al. (2009). Anticancer activity of CX-3543: a direct inhibitor of rRNA biogenesis. Cancer Res. *69*, 7653–7661.

Duffy, M.J. (2002). Urokinase-type plasminogen activator: a potent marker of metastatic potential in human cancers. Biochem. Soc. Trans. *30*, 207–210.

Dutra, F.F., and Bozza, M.T. (2014). Heme on innate immunity and inflammation. Front. Pharmacol. *5*, 115.

Eddy, J., Vallur, A.C., Varma, S., Liu, H., Reinhold, W.C., Pommier, Y., and Maizels, N. (2011). G4 motifs correlate with promoter-proximal transcriptional pausing in human genes. Nucleic Acids Res. *39*, 4975–4983.

Eskew, J.D., Vanacore, R.M., Sung, L., Morales, P.J., and Smith, A. (1999). Cellular protection mechanisms against extracellular heme. heme-hemopexin,

but not free heme, activates the N-terminal c-jun kinase. J. Biol. Chem. *274*, 638–648.

Faller, M., Matsunaga, M., Yin, S., Loo, J.A., and Guo, F. (2007). Heme is involved in microRNA processing. Nat. Struct. Mol. Biol. *14*, 23–29.

Ferreira, A., Balla, J., Jeney, V., Balla, G., and Soares, M.P. (2008). A central role for free heme in the pathogenesis of severe malaria: the missing link? J. Mol. Med. (Berl.) *86*, 1097–1111.

Ferreira, A., Marguti, I., Bechmann, I., Jeney, V., Chora, A., Palha, N.R., Rebelo, S., Henri, A., Beuzard, Y., and Soares, M.P. (2011). Sickle hemoglobin confers tolerance to Plasmodium infection. Cell *145*, 398–409.

Furuyama, K., Kaneko, K., and Vargas, P.D. (2007). Heme as a magnificent molecule with multiple missions: heme determines its own fate and governs cellular homeostasis. Tohoku J. Exp. Med. *213*, 1–16.

Glei, M., Klenow, S., Sauer, J., Wegewitz, U., Richter, K., and Pool-Zobel, B.L. (2006). Hemoglobin and hemin induce DNA damage in human colon tumor cells HT29 clone 19A and in primary human colonocytes. Mutat. Res. *594*, 162–171.

González, V., Guo, K., Hurley, L., and Sun, D. (2009). Identification and characterization of nucleolin as a c-myc G-quadruplex-binding protein. J. Biol. Chem. *284*, 23622–23635.

Gray, L.T., Vallur, A.C., Eddy, J., and Maizels, N. (2014). G quadruplexes are genomewide targets of transcriptional helicases XPB and XPD. Nat. Chem. Biol. *10*, 313–318.

Gray, L.T., Puig Lombardi, E., Verga, D., Nicolas, A., Teulade-Fichou, M.P., Londoño-Vallejo, A., and Maizels, N. (2019). G-quadruplexes sequester free heme in living cells. Cell Chem. Biol. *26*, 1681–1691.e5.

Gueron, G., De Siervi, A., Ferrando, M., Salierno, M., De Luca, P., Elguero, B., Meiss, R., Navone, N., and Vazquez, E.S. (2009). Critical role of endogenous heme oxygenase 1 as a tuner of the invasive potential of prostate cancer cells. Mol. Cancer Res. *7*, 1745–1755.

Guo, J.U., and Bartel, D.P. (2016). RNA G-quadruplexes are globally unfolded in eukaryotic cells and depleted in bacteria. Science *353*, aaf5371.

Hampel, S.M., Pepe, A., Greulich-Bode, K.M., Malhotra, S.V., Reszka, A.P., Veith, S., Boukamp, P., and Neidle, S. (2013). Mechanism of the antiproliferative activity of some naphthalene diimide G-quadruplex ligands. Mol. Pharmacol. *83*, 470–480.

Hanna, D.A., Harvey, R.M., Martinez-Guzman, O., Yuan, X., Chandrasekharan, B., Raju, G., Outten, F.W., Hamza, I., and Reddi, A.R. (2016). Heme dynamics and trafficking factors revealed by genetically encoded fluorescent heme sensors. Proc. Natl. Acad. Sci. USA *113*, 7539–7544.

Hänsel-Hertsch, R., Beraldi, D., Lensing, S.V., Marsico, G., Zyner, K., Parry, A., Di Antonio, M., Pike, J., Kimura, H., Narita, M., et al. (2016). G-quadruplex structures mark human regulatory chromatin. Nat. Genet. *48*, 1267–1272.

Hawksworth, D., Ravindranath, L., Chen, Y., Furusato, B., Sesterhenn, I.A., McLeod, D.G., Srivastava, S., and Petrovics, G. (2010). Overexpression of C-MYC oncogene in prostate cancer predicts biochemical recurrence. Prostate Cancer Prostatic Dis. *13*, 311–315.

Hedblom, A., Hejazi, S.M., Canesin, G., Choudhury, R., Hanafy, K.A., Csizmadia, E., Persson, J.L., and Wegiel, B. (2019). Heme detoxification by heme oxygenase-1 reinstates proliferative and immune balances upon genotoxic tissue injury. Cell Death Dis. *10*, 72.

Hou, Y., Okamoto, C., Okada, K., Kawao, N., Kawata, S., Ueshima, S., and Matsuo, O. (2007). c-Myc is essential for urokinase plasminogen activator expression on hypoxia-induced vascular smooth muscle cells. Cardiovasc. Res. *75*, 186–194.

Hu, M.H., Wu, T.Y., Huang, Q., and Jin, G. (2019). New substituted quinoxalines inhibit triple-negative breast cancer by specifically downregulating the c-MYC transcription. Nucleic Acids Res. *47*, 10529–10542.

Hvidberg, V., Maniecki, M.B., Jacobsen, C., Højrup, P., Møller, H.J., and Moestrup, S.K. (2005). Identification of the receptor scavenging hemopexin-heme complexes. Blood *106*, 2572–2579.

Jaworski, F.M., Gentilini, L.D., Gueron, G., Meiss, R.P., Ortiz, E.G., Berguer, P.M., Ahmed, A., Navone, N., Rabinovich, G.A., Compagno, D., et al. (2017).

In vivo hemin conditioning targets the vascular and immunologic compartments and restrains prostate tumor development. Clin. Cancer Res. *23*, 5135–5148.

Kosman, J., and Juskowiak, B. (2016). Hemin/G-quadruplex structure and activity alteration induced by magnesium cations. Int. J. Biol. Macromol. *85*, 555–564.

Kristiansen, M., Graversen, J.H., Jacobsen, C., Sonne, O., Hoffman, H.J., Law, S.K., and Moestrup, S.K. (2001). Identification of the haemoglobin scavenger receptor. Nature *409*, 198–201.

Larsen, R., Gozzelino, R., Jeney, V., Tokaji, L., Bozza, F.A., Japiassú, A.M., Bonaparte, D., Cavalcante, M.M., Chora, A., Ferreira, A., et al. (2010). A central role for free heme in the pathogenesis of severe sepsis. Sci. Transl. Med. *2*, 51ra71.

Lehrer, S. (2010). Association between malaria incidence and all cancer mortality in fifty U.S. States and the District of Columbia. Anticancer Res. *30*, 1371–1373.

Leonardi, D.B., Anselmino, N., Brandani, J.N., Jaworski, F.M., Páez, A.V., Mazaira, G., Meiss, R.P., Nuñez, M., Nemirovsky, S.I., Giudice, J., et al. (2019). Heme oxygenase 1 impairs glucocorticoid receptor activity in prostate cancer. Int. J. Mol. Sci. *20*, 1006.

Lin, T., Maita, D., Thundivalappil, S.R., Riley, F.E., Hambsch, J., Van Marter, L.J., Christou, H.A., Berra, L., Fagan, S., Christiani, D.C., and Warren, H.S. (2015). Hemopexin in severe inflammation and infection: mouse models and human diseases. Crit. Care *19*, 166.

McLuckie, K.I., Di Antonio, M., Zecchini, H., Xian, J., Caldas, C., Krippendorff, B.F., Tannahill, D., Lowe, C., and Balasubramanian, S. (2013). G-quadruplex DNA as a molecular target for induced synthetic lethality in cancer cells. J. Am. Chem. Soc. *135*, 9640–9643.

Michelotti, E.F., Tomonaga, T., Krutzsch, H., and Levens, D. (1995). Cellular nucleic acid binding protein regulates the CT element of the human c-myc protooncogene. J. Biol. Chem. *270*, 9494–9499.

Mulvaney, E.P., Shilling, C., Eivers, S.B., Perry, A.S., Bjartell, A., Kay, E.W., Watson, R.W., and Kinsella, B.T. (2016). Expression of the TPα and TPβ isoforms of the thromboxane prostanoid receptor (TP) in prostate cancer: clinical significance and diagnostic potential. Oncotarget *7*, 73171–73187.

Mungall, S., and Mathieson, P. (2002). Hemolytic uremic syndrome in metastatic adenocarcinoma of the prostate. Am. J. Kidney Dis. *40*, 1334–1336.

Murat, P., and Balasubramanian, S. (2014). Existence and consequences of G-quadruplex structures in DNA. Curr. Opin. Genet. Dev. *25*, 22–29.

Nassir, A.M. (2020). A piece in prostate cancer puzzle: Future perspective of novel molecular signatures. Saudi J. Biol. Sci. *27*, 1148–1154.

Nemeth, Z., Li, M., Csizmadia, E., Döme, B., Johansson, M., Persson, J.L., Seth, P., Otterbein, L., and Wegiel, B. (2015). Heme oxygenase-1 in macrophages controls prostate cancer progression. Oncotarget *6*, 33675–33688.

Neumann, C.A., Krause, D.S., Carman, C.V., Das, S., Dubey, D.P., Abraham, J.L., Bronson, R.T., Fujiwara, Y., Orkin, S.H., and Van Etten, R.A. (2003). Essential role for the peroxiredoxin Prdx1 in erythrocyte antioxidant defence and tumour suppression. Nature *424*, 561–565.

Paul, R., Das, T., Debnath, M., Chauhan, A., and Dash, J. (2020). G-quadruplex-binding small molecule induces synthetic lethality in breast cancer cells by inhibiting c-MYC and BCL2 expression. ChemBioChem *21*, 963–970.

Poon, L.C., Methot, S.P., Morabi-Pazooki, W., Pio, F., Bennet, A.J., and Sen, D. (2011). Guanine-rich RNAs and DNAs that bind heme robustly catalyze oxygen transfer reactions. J. Am. Chem. Soc. *133*, 1877–1884.

Qiu, J., Chen, S., Su, L., Liu, J., Xiao, N., Ou, T.M., Tan, J.H., Gu, L.Q., Huang, Z.S., and Li, D. (2014). Cellular nucleic acid binding protein suppresses tumor cell metastasis and induces tumor cell death by downregulating heterogeneous ribonucleoprotein K in fibrosarcoma cells. Biochim. Biophys. Acta *1840*, 2244–2252.

Qiu, J., Liu, J., Chen, S., Ou, T.M., Tan, J.H., Gu, L.Q., Huang, Z.S., and Li, D. (2015). Role of Hairpin-Quadruplex DNA Secondary Structural Conversion in the Promoter of hnRNP K in Gene Transcriptional Regulation. Org. Lett. *17*, 4584–4587.

Quigley, D.A., Dang, H.X., Zhao, S.G., Lloyd, P., Aggarwal, R., Alumkal, J.J., Foye, A., Kothari, V., Perry, M.D., Bailey, A.M., et al. (2018). Genomic hallmarks and structural variation in metastatic prostate cancer. Cell *174*, 758–769.e759.

Ramos, R., Lopes, F., Rodrigues, T., Rolim, N., Rodrigues, I., and Monteiro, H. (2013). Advanced prostate cancer presenting as hemolytic uremic syndrome. Case Rep. Urol. *2013*, 459618.

Rodriguez, R., Miller, K.M., Forment, J.V., Bradshaw, C.R., Nikan, M., Britton, S., Oelschlaegel, T., Xhemalce, B., Balasubramanian, S., and Jackson, S.P. (2012). Small-molecule-induced DNA damage identifies alternative DNA structures in human genes. Nat. Chem. Biol. *8*, 301–310.

Saito, K., Tai, H., Fukaya, M., Shibata, T., Nishimura, R., Neya, S., and Yamamoto, Y. (2012a). Structural characterization of a carbon monoxide adduct of a heme-DNA complex. J. Biol. Inorg. Chem. *17*, 437–445.

Saito, K., Tai, H., Hemmi, H., Kobayashi, N., and Yamamoto, Y. (2012b). Interaction between the heme and a G-quartet in a heme-DNA complex. Inorg. Chem. *51*, 8168–8176.

Sen, D., and Poon, L.C. (2011). RNA and DNA complexes with hemin [Fe(III) heme] are efficient peroxidases and peroxygenases: how do they do it and what does it mean? Crit. Rev. Biochem. Mol. Biol. *46*, 478–492.

Shariat, S.F., Roehrborn, C.G., McConnell, J.D., Park, S., Alam, N., Wheeler, T.M., and Slawin, K.M. (2007). Association of the circulating levels of the urokinase system of plasminogen activation with the presence of prostate cancer and invasion, progression, and metastasis. J. Clin. Oncol. *25*, 349–355.

Shibata, T., Nakayama, Y., Katahira, Y., Tai, H., Moritaka, Y., Nakano, Y., and Yamamoto, Y. (2016). Characterization of the interaction between heme and a parallel G-quadruplex DNA formed from d(TTGAGG). Biochim. Biophys. Acta Gen. Subj *1861*, 1264–1270.

Shumayrikh, N., Huang, Y.C., and Sen, D. (2015). Heme activation by DNA: isoguanine pentaplexes, but not quadruplexes, bind heme and enhance its oxidative activity. Nucleic Acids Res. *43*, 4191–4201.

Siddiqui-Jain, A., Grand, C.L., Bearss, D.J., and Hurley, L.H. (2002). Direct evidence for a G-quadruplex in a promoter region and its targeting with a small molecule to repress c-MYC transcription. Proc. Natl. Acad. Sci. USA *99*, 11593–11598.

Soares, M.P., and Hamza, I. (2016). Macrophages and iron metabolism. Immunity *44*, 492–504.

Straka, J.G., Rank, J.M., and Bloomer, J.R. (1990). Porphyria and porphyrin metabolism. Annu. Rev. Med. *41*, 457–469.

Takachi, R., Tsubono, Y., Baba, K., Inoue, M., Sasazuki, S., Iwasaki, M., and Tsugane, S.; Japan Public Health Center-Based Prospective Study Group (2011). Red meat intake may increase the risk of colon cancer in Japanese, a population with relatively low red meat consumption. Asia Pac. J. Clin. Nutr. *20*, 603–612.

Tassidis, H., Brokken, L.J., Jirström, K., Bjartell, A., Ulmert, D., Härkönen, P., and Wingren, A.G. (2013). Low expression of SHP-2 is associated with less favorable prostate cancer outcomes. Tumour Biol. *34*, 637–642.

Tolosano, E., Hirsch, E., Patrucco, E., Camaschella, C., Navone, R., Silengo, L., and Altruda, F. (1999). Defective recovery and severe renal damage after acute hemolysis in hemopexin-deficient mice. Blood *94*, 3906–3914.

Tolosano, E., Fagoonee, S., Hirsch, E., Berger, F.G., Baumann, H., Silengo, L., and Altruda, F. (2002). Enhanced splenomegaly and severe liver inflammation in haptoglobin/hemopexin double-null mice after acute hemolysis. Blood *100*, 4201–4208.

Tomonaga, T., and Levens, D. (1995). Heterogeneous nuclear ribonucleoprotein K is a DNA-binding transactivator. J. Biol. Chem. *270*, 4875–4881.

Travascio, P., Bennet, A.J., Wang, D.Y., and Sen, D. (1999). A ribozyme and a catalytic DNA with peroxidase activity: active sites versus cofactor-binding sites. Chem. Biol. *6*, 779–787.

Valencia, T., Kim, J.Y., Abu-Baker, S., Moscat-Pardos, J., Ahn, C.S., Reina-Campos, M., Duran, A., Castilla, E.A., Metallo, C.M., Diaz-Meco, M.T., and Moscat, J. (2014). Metabolic reprogramming of stromal fibroblasts through p62-mTORC1 signaling promotes inflammation and tumorigenesis. Cancer Cell *26*, 121–135.

van der Meer-van Kraaij, C., Kramer, E., Jonker-Termont, D., Katan, M.B., van der Meer, R., and Keijer, J. (2005). Differential gene expression in rat colon by dietary heme and calcium. Carcinogenesis *26*, 73–79.

Wegiel, B., Bjartell, A., Tuomela, J., Dizeyi, N., Tinzl, M., Helczynski, L., Nilsson, E., Otterbein, L.E., Härkönen, P., and Persson, J.L. (2008). Multiple cellular mechanisms related to cyclin A1 in prostate cancer invasion and metastasis. J. Natl. Cancer Inst. *100*, 1022–1036.

Wegiel, B., Gallo, D., Csizmadia, E., Harris, C., Belcher, J., Vercellotti, G.M., Penacho, N., Seth, P., Sukhatme, V., Ahmed, A., et al. (2013). Carbon monoxide expedites metabolic exhaustion to inhibit tumor growth. Cancer Res. *73*, 7009–7021.

Wegiel, B., Hauser, C.J., and Otterbein, L.E. (2015). Heme as a danger molecule in pathogen recognition. Free Radic. Biol. Med. *89*, 651–661.

Wyganowska-Świątkowska, M., Tarnowski, M., Murtagh, D., Skrzypczak-Jankun, E., and Jankun, J. (2019). Proteolysis is the most fundamental property of malignancy and its inhibition may be used therapeutically [Review]. Int. J. Mol. Med. *43*, 15–25.

Yamamoto, Y., Kinoshita, M., Katahira, Y., Shimizu, H., Di, Y., Shibata, T., Tai, H., Suzuki, A., and Neya, S. (2015). Characterization of heme-DNA complexes composed of some chemically modified hemes and parallel G-quadruplex DNAs. Biochemistry *54*, 7168–7177.

Yin, L., Wu, N., Curtin, J.C., Qatanani, M., Szwergold, N.R., Reid, R.A., Waitt, G.M., Parks, D.J., Pearce, K.H., Wisely, G.B., and Lazar, M.A. (2007). Rev-erbα, a heme sensor that coordinates metabolic and circadian pathways. Science *318*, 1786–1789.

Yuan, X., Rietzschel, N., Kwon, H., Walter Nuno, A.B., Hanna, D.A., Phillips, J.D., Raven, E.L., Reddi, A.R., and Hamza, I. (2016). Regulation of intracellular heme trafficking revealed by subcellular reporters. Proc. Natl. Acad. Sci. USA *113*, E5144–E5152.

Zhang, H., Alberich-Jorda, M., Amabile, G., Yang, H., Staber, P.B., Di Ruscio, A., Welner, R.S., Ebralidze, A., Zhang, J., Levantini, E., et al. (2013). Sox4 is a key oncogenic target in C/EBPα mutant acute myeloid leukemia. Cancer Cell *24*, 575–588.

Zhang, L., Ulstrup, J., and Zhang, J. (2016). Voltammetry and molecular assembly of G-quadruplex DNAzyme on single-crystal Au(111)-electrode surfaces - hemin as an electrochemical intercalator. Faraday Discuss. *193*, 99–112.

STAR★METHODS

KEY RESOURCES TABLE

REAGENT or RESOURCE	SOURCE	IDENTIFIER
Antibodies		
anti-BG4	Millipore-Sigma	Cat#: MABE1126
Rabbit polyclonal anti-HO1	Enzo Life Sciences	Cat#: ADI-OSA-110; RRID:AB_10617276
Rabbit monoclonal anti-Hemopexin	Abcam	Cat#: ab124935; RRID:AB_10975463
Mouse monoclonal anti-p63	DAKO	Cat#: M7317
Rabbit monoclonal anti-AMACR	DAKO	Cat#: M3616; RRID:AB_2305454
Rabbit anti-P(Ser780)-Rb	Cell Signaling	Cat#: 9307S; RRID:AB_330015
Mouse monoclonal anti-Rb	Cell Signaling	Cat#: 9309; RRID:AB_823629
Mouse monoclonal anti-HO-1	Enzo Laboratories	Cat#: ADI-OSA-110; RRID:AB_10617276
Rabbit monoclonal anti-P(Ser139)-H2AX (γH2AX)	Cell Signaling	Cat#: 9178; RRID:AB_2072132
anti-cyclin B1	Cell Signaling	Cat#: 4138
Mouse monoclonal anti-P(Ser1981)-ATM	Cell Signaling	Cat#: 4526S; RRID:AB_2072132
Mouse monoclonal anti-c-myc	Santa Cruz Biotechnology	Cat#: sc-40; RRID:AB_2857941
Rabbit anti-P-(Ser10)Histone H3	Cell Signaling	Cat#: 9711S; RRID:AB_331536
Mouse monoclonal anti-β-Actin	Sigma Aldrich	Cat#: A2228; RRID:AB_476697
Rabbit anti-lamin A/C	Cell Signaling	Cat#: 2032S; RRID:AB_2136278
Rabbit monoclonal anti- GAPDH	Cell Signaling	Cat#: 2118; RRID:AB_561053
anti-Nucleolin	Abcam	Cat#: AB13541; RRID:AB_300442
anti-NM23H2	Santa Cruz Biotechnology	Cat#: SC-100400; RRID:AB_1126689
anti-CNBP	Santa Cruz Biotechnology	Cat#: SC-515387 X
anti-hnRNPK	Abcam	Cat#: AB39975; RRID:AB_732981
Biological Samples		
TMA from radical prostatectomies of prostate cancer patients	Skåne University Hospital, Malmö, Sweden	N/A
Plasma from patients undergoing a PSA test	Skåne University Hospital, Malmö, Sweden	N/A
Chemicals, Peptides, and Recombinant Proteins		
Hemin	Sigma-Aldrich	Cat# 51280
GQC-05	Dr. Hurley's laboratory Brown et al., 2011 Brooks and Hurley, 2009	N/A
o-dianisidine dihydrochloride	Sigma-Aldrich	Cat# D3252
Critical Commercial Assays		
Nuclear/cytoplasmic fractionation kit	BioVision	Cat# K270
BCA Protein Kit	Pierce	Cat# 23227
Hemin Colorimetric Assay Kit	BioVision	Cat# K672
Human Hemopexin ELISA Kit	Abcam	Cat# ab108859
Deposited Data		
RNA sequencing data from PC3 cells untreated or treated with heme (50 μM) for 2 or 4 hours	Gene Expression Omnibus	GSE139091
Experimental Models: Cell Lines		
Prostate cancer PC3 cells	Dr. Steven Balk (BIDMC, Boston)	N/A
Prostate cancer TRAMP-C1 cells	ATCC	CRL-2730
Prostate cancer LnCaP cells	ATCC	CRL-1740

(Continued on next page)

Continued

REAGENT or RESOURCE	SOURCE	IDENTIFIER
Prostate epithelial cells PNT1A	Dr. Nishtman Dizeyi (Lund University, Malmo, Sweden)	N/A
Lung carcinoma A549 cells	ATCC	CCL-185
Human bronchial epithelial cells NHBE	Lonza	CC-2540S
Lewis lung carcinoma LLC cells	ATCC	CRL-1642
BJ fibroblasts (ELR, ELT and EHZ cells)	Dr. Weinberg Boehm et al., 2005	N/A
Experimental Models: Organisms/Strains		
Nude *nu/nu* mice	Jackson Laboratories	Stock No: 002019
C57Bl6/J Wild Type	Jackson Laboratories	Stock No: 000664
C57Bl6 Hx$^{-/-}$	Dr. Tolosano's laboratory Tolosano et al., 1999	N/A
Oligonucleotides		
C-MYC promoter FW: GCTGGAAACCTTGCACCTC	This paper	N/A
C-MYC promoter RV: CGTTCAGGTTTGCGAAAGTA	This paper	N/A
WT Pu27 for EMSA: TGGGGAGGGTGGGGAGGGTGGGGAAGG	Siddiqui-Jain et al., 2002	N/A
Mutated Pu27 for EMSA: TGAGTAGCGTGAGCAGAGTG CGTAACG	Siddiqui-Jain et al., 2002	N/A
Hmox1, mouse FW: CTCACTATGCAACTCTGTTGGAGG	This paper	N/A
Hmox1, mouse RV: GTCTGTAATCCTAGCTCGAA	This paper	N/A
ALAS1 FW: TCTTCCGCAAGGCCAGTCT	This paper	N/A
ALAS1 RV: TGGGCTTGAGCAGCCTCTT	This paper	N/A
ZNF469 FW: CGCGAAGACCTTCCTGTTAG	This paper	N/A
ZNF469 RV: CTCTGTGATGAGGCTGTCCA	This paper	N/A
Hmox1, human/mouse FW: CAGGATTTGTCAGAGGCCCTGAAGG	This paper	N/A
Hmox1, human/mouse RV: TGTGGTACAGGGAGGCCATCACC	This paper	N/A
c-MYC human FW: 5'ATGAAAAGGCCCCCAAGGTAGTTATCC	This paper	N/A
c-MYC human RV: 5'GTCGTTTCCGCAACAAGTCCTCTTC	This paper	N/A
c-MYC, mouse FW: GCCCAGTGAGGATATCTGGA	This paper	N/A
c-MYC, mouse RV: ATCGCAGATGAAGCTCTGGT	This paper	N/A
MMP2, human FW: CGGCCGCAGTGACGGAAA	This paper	N/A
MMP2, human RV: CATCCTGGGACAGACGGAAG	This paper	N/A
MMP2, mouse FW: GTCGCCCCTAAAACAGACAA	This paper	N/A
MMP2, mouse RV: GGTCTCGATGGTGTTCTGGT	This paper	N/A
MMP9, human FW: TTGACAGCGACAAGAAGTGG	This paper	N/A
MMP9, human RV: GCCATTCACGTCGTCCTTAT	This paper	N/A
MMP9, mouse FW: CGTCGTGATCCCCACTTACT	This paper	N/A
MMP9, mouse RV: AACACACAGGGTTTGCCTTC	This paper	N/A
uPA, human FW: CAGGGCATCTCCTGTGCATG	This paper	N/A
uPA, human RV: AGCCCTGCCCTGAAGTCGTTA	This paper	N/A
uPA, mouse FW: GCCTGCTGTCCTTCAGAAAC	This paper	N/A
uPA, mouse RV: TAGAGCCTTCTGGCCACACT	This paper	N/A
AMIGO2, human FW: TCGTTTGCAAAGCTGAACAC	This paper	N/A
AMIGO2, human RV: GCAGAAGCACTTCCAGAACC	This paper	N/A
AMIGO2, mouse FW: TCACGGGAACCCATTTGTAT	This paper	N/A
AMIGO2, mouse RV: CTGAGCCTCGTGGATAAAGC	This paper	N/A
ULK1, human FW: CAGAACTACCAGCGCATTGA	This paper	N/A
ULK1, human RV: TCCACCCAGAGACATCTTCC	This paper	N/A

(Continued on next page)

Continued		
REAGENT or RESOURCE	SOURCE	IDENTIFIER
ULK1, mouse FW: CCCAGAGTACCCGTACCAGA	This paper	N/A
ULK1, mouse RV: GTGTAGGGTTTCCGTGTGCT	This paper	N/A
Software and Algorithms		
Differential gene expression analysis	This paper	https://combine-australia.github.io/RNAseq-R/06-rnaseq-day1.html

RESOURCE AVAILABILITY

Lead Contact
Further information and requests for resources and reagents should be directed to and will be fulfilled by the Lead Contact, Dr. Barbara Wegiel (Department of Surgery, Beth Israel Deaconess Medical Center, Harvard Medical School, bwegiel@bidmc.harvard.edu).

Materials Availability
This study did not generate any unique reagents.

Data and Code Availability
RNaseq data generated in this study were deposited on Gene Expression Omnibus under the accession number: GSE139091 (a private access token is ubmlmigqzlkrdiv, https://www.ncbi.nlm.nih.gov/geo/query/acc.cgi?acc=GSE139091).

EXPERIMENTAL MODEL AND SUBJECT DETAILS

Cell lines
Prostate cancer PC3 cells were a gift from Dr. Steven Balk (BIDMC, Boston, MA) and were maintained in RPMI medium (GIBCO, Life Technologies) supplemented with 10% Fetal Bovine Serum (Atlanta Biologicals). TRAMP-C1 cells were purchased from ATCC and maintained in DMEM supplemented with 10% Fetal Bovine Serum (Atlanta Biologicals). PC3 Control shRNA or PC3 shRNA c-*myc* (Addgene), LNCaP, A549 and PNT1A were previously described (Wegiel et al., 2013). BJ fibroblasts transformed with oncogenes (ELR, ELT, EHZ) were kindly provided by Dr. Weinberg (MIT, Cambridge, MA) (Boehm et al., 2005) and were cultured in DMEM high glucose supplemented with 10% FBS. Human bronchial epithelial cells (NHBE) were from Lonza and were maintained in Bronchial Epithelial Cell Growth Medium with Supplements as specified by manufacturer's protocol (Lonza). Cells were maintained in a 37°C humidified incubator with 5% CO_2 and 21% O_2.

Patients samples
Tissues from radical prostatectomies of 341 prostate cancer patients, operated between 1998 and 2006 at Skåne University Hospital, Malmö, Sweden was used to construct a tissue microarray (TMA) as previously described in (Tassidis et al., 2013). Clinical follow-up data of minimum 10 years and pathological staging was available for most of the patients and the clinical characteristics have been previously described in Mulvaney et al. (2016). Plasma samples were from patients undergoing a PSA test at the Malmö University Hospital between 2004 and 2010 (ethical permit number 2016/1030). The patients were followed up for a minimum of 8 years. All patients included in this study received a prostate cancer diagnosis after the PSA test, based on positive biopsies. Patients who received a diagnosis of Gleason score 6 or 7 were defined as "low grade" (n = 16, mean age 72.7) and those with a diagnosis of Gleason score 8 or higher were defined as "high grade" (n = 10, mean age 70.8). Healthy donors were men with no known cancer diagnosis (n = 7, mean age 57,1) who volunteered to donate blood at the Malmö University Hospital (ethical permit 2019/02234). The blood was collected in EDTA tubes and centrifuged for 10 minutes at 2000 x g. Plasma was extracted, aliquoted and stored at −80°C until further use.

Animal models
Nude *nu/nu* mice and C57Bl6 mice were from Jackson Laboratories. $Hx^{-/-}$ mice were from Tolosano et al. 1999, (2002). For prostate studies only male mice were used. All animals were kept in ventilated cages (up to five mice per cage) in a 12-hour light-dark cycle and were provided water and food *ad libitum* at all times. The procedures were approved by the Institutional Animal Care and Use Committees at Beth Israel Deaconess Medical Center.

METHOD DETAILS

Reagents
Fe (III) heme (hemin; referred as 'heme' throughout the text) (Sigma-Aldrich) was prepared by dissolving powder in 0.1 N NaOH and then titrated with 0.1 N HCl to biological pH 7.4, followed by adjustment to the final concentration (10 mM) with saline. Heme stock

was then aliquoted and frozen at $-80°C$ until use; each aliquot was thawed only once. Experiments utilizing heme were carried out in the dark at various concentration of 1-50 μM. GQC-05 (Dr. Hurley's laboratory) was previously described (Brooks and Hurley, 2009; Brown et al., 2011) and used at 10 μM concentration for treatment *in vitro*.

Soft agar colony assay

$1^\times10^4$ PC3 cells were suspended in 0.35% biotechnology grade agarose (Amresco) in RPMI supplemented with 10% FBS and plated before solidifying on a solid 0.5% agarose with RPMI medium supplemented with 10% FBS. Medium was replaced every third day. Colonies were maintained for 2-3 weeks in a humidified incubator at 37°C, followed by staining with methylene blue (Sigma-Aldrich) and counting individually.

Cell cycle analysis

For cell cycle analysis, cells were serum starved for 48 h and then treated with 50 μM heme for additional 8-48 h. Cells were harvested and washed in PBS and then fixed in 70% cold ethanol while vortexing. Cells were fixed for at least 30 min at 4°C. After fixation, cells were washed twice in PBS and resuspended in PBS with RNase (100 μg /ml). Cells were stained with propidium iodide (50 μg/ml) and analyzed by flow cytometry.

Tumor models

Nude *nu/nu* mice (Jackson Laboratories, Stock No: 002019) were injected subcutaneously with $5x10^6$ PC3 prostate cancer cells in each of two flanks per animal. Once tumors were established, mice were injected with heme (35 mg/kg, *i.p.*) once daily for an additional two weeks. Tumor sizes were monitored by caliper. LLC tumors were established in C57Bl6/J mice (Jackson Laboratories, Stock No: 000664) by injecting of $0.5x10^6$ Lewis lung carcinoma cells subcutaneously. Tumors were established in 10-14 days and mice were treated with heme (35 mg/kg, *i.p.*) once daily for an additional week. TRAMP-C1 tumors were established by injecting of $2x10^6$ cells in the prostate of the animals. Tumors were established for 1 week and mice were treated with heme (35 mg/kg, *i.p.*) once daily for 4 additional weeks. Tumors were isolated and their sizes were measured by caliper.

BG4 antibody generation

BG4 antibody encoding plasmid (Biffi et al., 2013) was a kind gift of Dr. Balasubramanian Lab (Cambridge University, UK). The single chain antibody was modified at the Creative Biolabs to generate a human IgG encoding plasmid and transfected into HEK293 cells, after which the product was purified by HiTrap rProteinG FF and filtered by 0.2 μm. The antibody was aliquoted and frozen at $-20°C$ or $-80°C$ until use.

IHC and immunostaining

For IHC on TMA, deparaffinized 4-μm sections from the TMA blocks were subjected to antigen retrieval using a PT-Link module (Dako, Glostrup, Denmark) at 95–99°C for 20 min in citric acid buffer (0.01 M, pH 6.0). Immunostaining for BG4 (1:300, Millipore), HO-1 (1:400, Stressgen) and hemopexin (1:500, Abcam) was performed using EnVision Flex high-pH reagent (Dako) in an Autostainer Plus system according to manufacturer's protocol. In order to distinguish benign from tumor areas, consecutive sections of the TMAs were also stained for p63 (M7001, 1:50 DAKO) and AMACR (alpha-methyl acyl-CoA racemase; M3616, 1:100 DAKO) respectively. Gleason score was assigned to each TMA core by a senior National Board certified pathologist with help of hematoxylin & eosin (H&E) stained tissue sections. The slides were digitized on an Aperio Scanscope scanner and visualized on the Aperio ImageScope software (Leica Biosystems, Wetzlar, Germany). Immunostained sections were scored considering the intensity of the staining and also the percentage of stained cells. Samples were given an intensity score between 0 and 3 (0 = negative, 1 = low, 2 = moderate, 3 = high) and a positivity score based on the percentage of stained cells (< 10% = 1, 11%–75% = 2, > 75% = 3). These two scores (intensity score and fraction of positively stained cells) were then multiplied to give a final expression score (H-score, 0-9). Two benign and two cancer cores from each patient were available and results are based on the average value for the two cores. The total number of cores analyzed is reported in Table S4.

Immunohistochemistry of paraffin embedded formalin fixed tissues was performed as previously described (Wegiel et al., 2013). Slides containing either FFPE sections or cells underwent a rehydration procedure, followed by high pressure-cooking antigen retrieval method in citrate buffer, blocking with 7% horse serum (Vector Laboratories) and overnight incubation with primary antibodies at 4°C. After washing with PBS, slides were blocked with H_2O_2 followed by incubation with either Alexa Fluor conjugated secondary antibodies (Thermo Scientific) or biotin-labeled secondary antibodies (Vector Laboratories) for 1 h at RT. For immunofluorescence, slides were then contrast stained with Hoechst, dried, and mounted with gelvatol. For light microscopy, Vectastain Elite ABC System was used to enhance the signals (Vector Laboratories) for 30 minutes followed by reaction development with DAB Substrate (Vector Laboratories).

Nuclear/Cytoplasmic Fractionation

Fractions were isolated using the nuclear/cytoplasmic fractionation kit (BioVision) according to manufacturer's protocol. Briefly, cells were trypsinized, washed once with PBS, and incubated on ice for 10 minutes with cytosolic extraction buffer A after which cytosolic extraction buffer B was added, vortexed, and then placed on ice for 1 minute. After centrifugation, the clear supernatant was removed

as the cytoplasmic fraction, while the pellet was washed once with PBS and then resuspended in Nuclear Extraction buffer A followed by sonication to ensure nuclear fraction lysis.

Immunoblotting

Proteins were harvested in lysis buffer (25 mM Tris-HCl, 150 mM NaCl, 1% NP-40, 100 mM NaF, 1 Complete Mini Protease Inhibitor Cocktail Tablet (Roche)). After sonication, lysates were centrifuged at 12,000 x g at 4° for 10 minutes. Protein concentrations were measured using the BCA Protein Kit (Pierce). 15-35 μg proteins were applied on 4%–12% NuPAGE Bis-Tris SDS polyacrylamide gel electrophoresis in MES SDS running system (Novex by Life Technologies) followed by transfer to PVDF membrane (Amersham and Biorad). Following transfer, membranes were blocked in 5% nonfat milk for one hour. The following antibodies were applied rotating overnight at 4°C: P-(Ser780)-Rb (Cell Signaling), Rb (Cell Signaling), HO-1 (Enzo Laboratories), HO-1 rabbit monoclonal (Abcam), P-(Ser139)-H2AX (γH2AX) (Cell Signaling), cyclin B1 (Santa Cruz Biotechnology), P-(Ser1981)-ATM (Cell Signaling), c-myc (Santa Cruz Biotechnology), and P-(Ser10)Histone H3 (Cell Signaling). β-Actin (Sigma Aldrich) was used for total lysates while lamin A/C and GAPDH (Cell Signaling Technologies) were used for nuclear and cytoplasmic loading controls, respectively. The following day, after brief washing with Tris-buffered saline, membranes were incubated with HRP conjugated secondary antibodies (Cell Signaling Technologies), followed by chemiluminescent (ECL, Thermo Fisher) detection on film (Bioexpress) or by Chemi Chemi-Doc™ Touch Imaging System (Bio-Rad).

Chromatin immunoprecipitation (ChIP):

ChIP was performed as previously described by Zhang et al. (2013). Briefly, treated and untreated PC3 cells were washed twice with PBS and then crosslinked with 1% formaldehyde. Cell pellets were washed twice with ice-cold 1X PBS (freshly supplemented with 1 mM PMSF). Pellets of 3 x10^6 cells were used for immunoprecipitation and lysed for 10 minutes on ice and chromatin fragmented using a Bioruptor Model 300, Diagenode (20 cycles, 30 s on, 60 s off, high power). Each ChIP was performed with 1 to 8 μg of the following antibodies: anti-Nucleolin (Abcam), anti-NM23H2 (Santa Cruz Biotechnology), anti-hnRNPK (Abcam), anti-CNBP (Santa Cruz Biotechnology), normal mouse IgG (Millipore 12-371b), and then incubated overnight at 4°C. A slurry of protein G magnetic beads (NEB) was used to capture enriched chromatin, which was then washed before reverse-crosslinking and proteinase K digestion at 65°C. Beads were then removed in the magnetic field and RNase treatment (5μg/μl Epicenter MRNA092) performed for 30 minutes at 37°C. ChIP DNA was extracted with Phenol:chloroform:isoamyl Alcohol 25:24:1, pH:8 (Sigma) and then precipitated with equal volume of isopropanol in presence of glycogen. DNA pellet was dissolved in 30μl of TE buffer for following qPCR analyses.

ChIP with flagged BG4 antibody (Millipore), was performed in the same conditions of lysis buffer and shering chromatin. 2 to 10 μg of antibody were initially incubated with the lysate at 4°C, O/N and then Anti-FLAG M2 Magnetic Beads (Sigma) were used to capture the fragmeted chromatin as previously described (Zhang et al., 2013). DNA isolated samples were all analyzed by quantitative real time PCR using the following primers: (c-MYC promoter) F: 5′ GCTGGAAACCTTGCACCTC, R: 5′ CGTTCAGGTTTGCGAAAGTA. Fold enrichment was calculated using the formula 2 (-ΔΔCt (ChIP/non-immune serum)).

RNA-sequencing

RNA was isolated from PC3 cells lysed in TRIzol reagent after treatment with heme for 2 or 4 hours. Biological duplicates were prepared. RNA quality was assessed using Bioanlyzer. Libraries were prepared using Illumina Truseq stranded Kit and sequenced on a BGI-SEQ, PE100 resulting in libraries with 40M reads per sample.

Oligonucleotides, EMSA and Circular Dichroism

Oligonucleotides (Life Technologies) were purified by 15% denaturing polyacrylamide gel electrophoresis followed by elution in water and ethanol precipitation overnight. Oligonucleotides were then end labeled with [γ-32P] ATP (Perkin Elmer) and T4 polynucleotide kinase (Roche/Sigma) and then passed through G-25 columns to remove unlabeled oligonucleotides. Labeled oligos were folded in 10 mM Tris-HCl pH 7.4 with or without 100 mM KCl in a PCR machine (BioRad) according to the following protocol: 95°C for 5 minutes, followed by slow cooling to 26°C over 1.5 hours. Binding reactions with or without IgG or BG4 antibodies were carried out using the Active Motif GelShift system of binding, stabilizing and dilution buffers (Active Motif) and run on 6% polyacrylamide gel. The gel was then dried and exposed to X-ray film and/or PhosphorImager screens. Oligonuclotides sequences used are as follows: Pu27 5′TGG GGA GGG TGG GGA GGG TGG GGA AGG 3′, Mutated Pu27 5′ TGA GTA GCG TGA GCA GAG TGC GTA ACG 3′ (Siddiqui-Jain et al., 2002). Circular dichroism and characterization of the melting temperature of the G4:heme complexes were performed as previously described (Siddiqui-Jain et al., 2002).

Real time PCR

RNA was isolated from snap-frozen tissues or cells (QIAGEN) according to manufacturer's protocol and eluted with water. 1 μg of isolated RNA, measured using Nanodrop, was then used to make cDNA using the iScript Reverse Transcription Supermix (BioRad) in 20 μl reaction. 1 μl of the undiluted cDNA was then used with SYBR green PCR Master Mix (Bio-Rad). Primer used were as follows:

Hmox1, mouse FW: CTCACTATGCAACTCTGTTGGAGG; RV: GTCTGTAATCCTAGCTCGAA; *Hmox1*, human/mouse FW: CAGG ATTTGTCAGAGGCCCTGAAGG; RV: TGTGGTACAGGGAGGCCATCACC; *c-MYC* human FW: 5'ATGAAAAGGCCCCCAAG GTAGTTATCC; RV: 5'GTCGTTTCCGCAACAAGTCCTCTTC; *c-MYC*, mouse FW: GCCCAGTGAGGATATCTGGA, RV: ATCGCAGAT GAAGCTCTGGT; *MMP2*, human FW: CGGCCGCAGTGACGGAAA, RV: CATCCTGGGACAGACGGAAG; *MMP2*, mouse FW: GTCGCCCCTAAAACAGACAA, RV: GGTCTCGATGGTGTTCTGGT; *MMP9*, human FW: TTGACAGCGACAAGAAGTGG, RV: GCCATTCACGTCGTCCTTAT; *MMP9*, mouse FW: CGTCGTGATCCCCACTTACT, RV: AACACACAGGGTTTGCCTTC; *uPA*, human FW: CAGGGCATCTCCTGTGCATG, RV: AGCCCTGCCCTGAAGTCGTTA; *uPA*, mouse FW: GCCTGCTGTCCTTCAGAAAC, RV: TAGAGCCTTCTGGCCACACT; *AMIGO2*, human FW: TCGTTTGCAAAGCTGAACAC, RV: GCAGAAGCACTTCCAGAACC; *AMIGO2*, mouse FW: TCACGGGAACCCATTTGTAT, RV: CTGAGCCTCGTGGATAAAGC; *ULK1*, human FW: CAGAACTACCAGCGCATTGA, RV: TCCACCCAGAGACATCTTCC; *ULK1*, mouse FW: CCCAGAGTACCCGTACCAGA, RV: GTGTAGGGTTTCCGTGTGCT; *ZNF469*, human/mouse FW: CGCGAAGACCTTCCTGTTAG, RV: CTCTGTGATGAGGCTGTCCA; *ALAS1*, FW: TCTTCCGCAAGGC CAGTCT, RV: TGGGCTTGAGCAGCCTCTT.

Viability assay
Cell viability was measured as previously described (Hedblom et al., 2019). Briefly, 2000 cells were plated in a 96 well plate and treated with increasing concentrations of GQC-05. After incubation, cells were stained with Crystal Violet solution (Sigma-Aldrich) for 20 min at room temperature and then extensively washed in double-distilled water. Wells were dried and 10% acetic acid was added to each well to dissolve the staining. The absorbance was measured at 560 nm using an ELISA plate reader.

Geo Profiles
GEO profiles from 18 normal prostatic tissues (without any pathological alterations), 62 tissues adjacent to tumors, 64 primary tumors and 24 metastatic samples were obtained from patients with prostate cancer as described in previously published data (Chandran et al., 2007; Nemeth et al., 2015). Metastatic biopsies were derived from patients with prostate cancer metastases to the liver, lymph nodes, kidney, lung and adrenal glands.

Heme and hemopexin measurement
Heme levels were measured using colorimetric kit following manufacturer protocol (Biovision). All experiments were also repeated using benzidine staining. The o-dianisidine stock solution was prepared (o-dianisidine: 60mg and 0.3 mL glacial acetic acid, 29.7 mL water) and used for staining immediately after mixing with 30% hydrogen peroxide. This working solution was added to the lysate in a proportion of 1:10. The absorbance of the colorimetric reaction was read by ELISA plate reader at 570 nm. In alternative method, cells seeded on the glass coverslips were stained with working solution followed by extensive washing and fixation with PFA and staining of the nuclei with hematoxylin. Hemopexin levels were measured using a colorimetric ELISA kit (Abcam ab108859) following manufacturer's protocol.

QUANTIFICATION AND STATISTICAL ANALYSIS

RNA-seq bioinformatics analyses
Raw fastq files first had optical duplicates removed using clumpify from the BBTools suite using the flag "dedupe spany addcount." Next, adaptor trimming was performed using bbduk, also from the BBTools suite using the flag "ktrim=l hdist=2." Next, reads were quality trimmed with Trimmomatic in paired end mode with the flags "ILLUMINACLIP: <adapter_path> Truseq3.PE.fa:2:15:4:4:true LEADING:20 TRAILING:20 SLIDINGWINDOW:4:15 MINLEN:25." Alignment was performed using STAR with the flags "–outFilter-ScoreMinOverLread 0.1–outFilterMatchNminOverLread 0.1–outFilterMultimapNmax 1" with the resultant bam files sorted and indexed using samtools. BamCoverage was used to generate coverage maps using default parameters. HTSeqCount was used to generate gene counts values using the flags "–stranded=no–mode=intersection-nonempty.

Differential Gene Expression, Pathway and Gene Set Enrichment Analysis
Differential gene expression analysis was performed following an available tutorial (https://combine-australia.github.io/RNAseq-R/06-rnaseq-day1.html). Briefly, cpm counts were calculated and genes with cpm values < 0.5 were excluded. Normalization factors were then calculated for TMM normalization. Differential expression was calculated using limma-voom using appropriate design matrices. Finally, appropriate contrasts were applied, and differential gene expression tables generated for the appropriate test conditions. Differential gene expression lists were then uploaded to QIAGEN's Ingenuity Pathway Analysis suite and analyzed online. Ranked gene lists based on the differential gene expression lists were used for Gene Set Enrichment Analysis using the Broad Institute tool.

Statistics

All data are presented as mean ± standard error of the mean (SEM) unless otherwise indicated. Statistical analysis was performed using one-way or two-way analysis of variance (ANOVA) followed by the post hoc Tukey or Bonferroni test or using unpaired T student test using Prism Graphpad and Excel software. Differences between groups were rated significant at values of $p < 0.05$. Kaplan-Meier survival curve analysis was performed in SPSS (IBM, USA). Median value was used to dichotomize the data into "low" and "high." Cox regression was used to determine hazard ratios, confidence intervals and p value. Details on the statistical method used are reported in each figure legend.